Mathematical Biosciences 262 (2015) 182–197

Contents lists available at ScienceDirect

Mathematical Biosciences

journal homepage: www.elsevier.com/locate/mbs

Robust global identifiability theory using potentials—Application to compartmental models

N. Wongvanich, C.E. Hann*, H.R. Sirisena

Department of Electrical and Computer Engineering, University of Canterbury, Private Bag 4800, Christchurch, New Zealand

ARTICLE INFO

Article history:
Received 8 April 2014
Revised 31 December 2014
Accepted 5 January 2015
Available online 4 February 2015

Keywords:
Identifiability
Potential jet space
Compartmental model
Parameter identification

ABSTRACT

This paper presents a global practical identifiability theory for analyzing and identifying linear and nonlinear compartmental models. The compartmental system is prolonged onto the potential jet space to formulate a set of input–output equations that are integrals in terms of the measured data, which allows for robust identification of parameters without requiring any simulation of the model differential equations. Two classes of linear and non-linear compartmental models are considered. The theory is first applied to analyze the linear nitrous oxide (N_2O) uptake model. The fitting accuracy of the identified models from differential jet space and potential jet space identifiability theories is compared with a realistic noise level of 3% which is derived from sensor noise data in the literature. The potential jet space approach gave a match that was well within the coefficient of variation. The differential jet space formulation was unstable and not suitable for parameter identification. The proposed theory is then applied to a nonlinear immunological model for mastitis in cows. In addition, the model formulation is extended to include an iterative method which allows initial conditions to be accurately identified. With up to 10% noise, the potential jet space theory predicts the normalized population concentration infected with pathogens, to within 9% of the true curve.

1. Introduction

The approach of *in silico* trials is very useful for testing new algorithms and models before implementation in a clinical environment and helps to generate novel predictions and hypotheses that enhance understanding of complex pharmacological systems [15]. A number of parameters characterizing the behavior of these systems are generally not accessible to direct measurement. Their values are thus approximated indirectly as a parameter identification problem [6]. Many biological, physiological and pharmacological systems are adequately described using first order, non-linear differential equations models describing the internal structure of the systems. A commonly used approximation that often suffices to capture the underlying dynamics is linear compartmental models [29].

Structural identifiability is an important prerequisite for the parameter estimation. If the models are not identifiable, any numerical optimization approach that seeks to find the parameters from measured data will be ill-conditioned and will not give physiologically consistent and accurate answers. Thus, the resulting estimate would not be reliable for *in silico* experiments. However, identifiability analyses can provide insight into the design of suitable experiments to provide unique identifiability and combined with *in silico* testing can provide guidelines or protocols for expensive or difficult *in vivo* experiments [7,24].

Identifiability analyses have been formalized by Bellman and Astrom for linear compartmental models [9]. The early theories of identifiability analyses concentrate on the similarity transform of the state matrix, and testing the rank of this transform [20,39]. Other approaches have used the Laplace transform of the input and output for identifiability [19,40,43].

Different approaches to the non-linear identifiability problem have been proposed in the literature, for example the Pohjanpalo Taylor series method [34], and the differential algebra based method [5,10,27,30,32]. Sedoglavic [37] constructs the variational system from the differential equation model to compute the required Jacobians to test for local algebraic observability. Karlssson [27] developed an efficient method for local structural identifiability analysis of very large scale systems, through a computation of random integer coefficient power series. The differential algebra based method is becoming more widely used due to its usefulness in addressing global as well as local models. Algorithms have been successfully developed and implemented in a range of available software packages [2,10,27,30]. In addition, probabilistic approaches have been developed and implemented [35,36]. Once structural identifiability has been determined, algorithms for parameter estimation in models of dynamical systems

* Corresponding author. Tel.: +64 3 364 2987x7242.
E-mail addresses: wongvanich@ieee.org (N. Wongvanich), chris.hann@canterbury.ac.nz (C.E. Hann), harsha.sirisena@canterbury.ac.nz (H.R. Sirisena).

http://dx.doi.org/10.1016/j.mbs.2015.01.013
0025-5564/

given discrete time measurement data can be applied. A survey on such algorithms is given in Ref. [44].

The current linear and non-linear global differential identifiability theories only address the existence of a unique set of parameters that match any given data set described by the model. In other words, the theory used to prove global identifiability gives no means to identify the parameters once the model is shown to be identifiable. The major problem is that differentials are very sensitive to noise so the formulation cannot be applied to real data [11]. Note that the profile likelihood approach developed by Raue *et al.* [35] provides a method to identify confidence interval estimates of the parameters from measured data, but only proves local identifiability and requires numerous computations in the solution domain.

This work presents a practical implementable approach to global identifiability theory by prolongation of the original compartmental differential equation models onto the potential jet space. This method allows the input–output equations to be formulated entirely in terms of integrals, so that measured data can be transformed on to the potential jetspace surface and parameter identification achieved without requiring any numerical solution of the underlying model. In other words, all computations are performed on the potential jet space which is highly efficient computationally and robust to noise. For the special case of the first order, minimal model of glucose–insulin dynamics, the method provides the mathematical foundation behind the previously developed integral method which has been used extensively in critical care [22]. The proposed theory is applied to a number of compartmental systems and provides both a theory for identifiability and a direct method for system identification. This method is shown to be robust to noise and thus suitable for practical modeling and experimental design.

2. Methodology

2.1. Differential Jet space

Differential equations, from a group transformations point of view, act on the space co-ordinatized by the dependent and independent variables. These group transformations give rise to the differential jet space, which forms the basis of most of the current approaches of identifiability analysis, since their actions are essentially the prolongation of the set of differential equations onto the differential jet space. This section gives an overview of the transformations and functions as well as the definition of the differential jet space [33].

A simple system of differential equation involves one independent variable t (time) on T, and q dependent variables (states) $x = (x_1, \ldots, x_q)$ as coordinates on $X \simeq \mathbb{R}^q$. The total space is the Euclidean space $E = T \times X \simeq \mathbf{R}^{1+q}$ coordinatized by the independent and dependent variables.

Definition 1. The total space $E = T \times X \simeq \mathbb{R}^1 \times \mathbb{R}^q$ the nth differential jet space $J^n = J^n E = T \times X^{(n)}$ is the Euclidean space of dimension $1 + q^{(n)} = 1 + q\binom{1+n}{n}$, whose co-ordinates consist of the time t, the q dependent variables x_α, and the derivative co-ordinates defined:

$$x^J_\alpha = \frac{d}{dt^\alpha} f^\alpha(t), \quad \alpha = 1, \ldots, q. \tag{1}$$

Definition 2. A smooth function $x = f(t)$ from T to X has nth prolongation $x^{(n)} = f^{(n)}(t)$, which is a function from T to $X^{(n)}$ obtained by evaluating all derivatives of f up to order n. The individual coordinate function of $f^{(n)}(t)$ is given by Eq. (1).

As an example, consider a simple map $f : T \to X, t \mapsto x = f(t)$, which maps the T axis onto the X axis. A 0-jet is given simply by its graph $(t, f(t))$. A 1-jet is given by the co-ordinate $(t, f(t), \dot{f}(t))$. A 2-jet is given by $(t, f(t), \dot{f}(t), \ddot{f}(t))$, and so on up to the n-jet. The set of all k-jets from T to X is called the k-jet space.

Formally, in terms of equivalence classes of section s in smooth vector bundle π, defined by $[s]^k_t$, the k-jet space is defined [25]:

$$J^k(\pi) = \{[s]^k_t : t \in T, s \in \Gamma(\pi)\} \tag{2}$$

The k-jet space is endowed with a smooth manifold structure, which is called the manifold of k-jets of sections of π and the following maps defined:

$$\pi_k : J^k(\pi) \to T, \quad [s]^k_t \to t \tag{3}$$

$$\pi_{k,l} : J^k(\pi) \to J^l(\pi), \quad [s]^k_t \to [s]^l_t, \quad k \geq l \tag{4}$$

are smooth fiber bundles. Eqs. (3) and (4) make it possible to write a given differential equation on sections of a bundle in an invariant form [25]. Most of the analyses of jet spaces focus on the case where $k = \infty$, that is, the space of $J^\infty(\pi)$, which is understood to be the limit of the chain:

$$\cdots \to J^{k+1}(\pi) \overset{\pi_{k+1,k}}{\to} J^k(\pi) \to \cdots \to J^1(\pi) \overset{\pi_{1,0}}{\to} J^0(\pi) \tag{5}$$

2.1.1. Geometric interpretation of the differential jet space

As an aid to understanding the differential jet space, this section gives numerical examples to demonstrate the geometric aspects in the differential jet space.

Consider the first order differential equations defined:

$$\dot{y} - y = 0, \quad y(0) = 1 \tag{6}$$

$$\dot{y} + y^2 = 0 \quad y(0) = 1 \tag{7}$$

The analytical solutions of Eqs. (6) and (7) are defined:

$$y(t) = \exp(t) \tag{8}$$

$$y(t) = \frac{1}{t+1} \tag{9}$$

Eqs. (6) and (7) represent a plane and parabolic surface respectively in the 1-jet space $(t, y, \dot{y})$ and are plotted in Figs. 1 and 2. The solutions of Eqs. (8) and (9) for a given initial condition are plotted as blue dashed curves on the (t, y) plane and their corresponding prolongation to the 1-jet space are the 3D space curves denoted by black lines. In theory, any measured data could be represented on the surfaces of Figs. 1 and 2 without having to solve the equations, but requires differentiation, which is sensitive to noise. The 1-jet space surfaces consist of the prolongated solutions of Eqs. (8) and (9) for all initial conditions $y(0) \in$

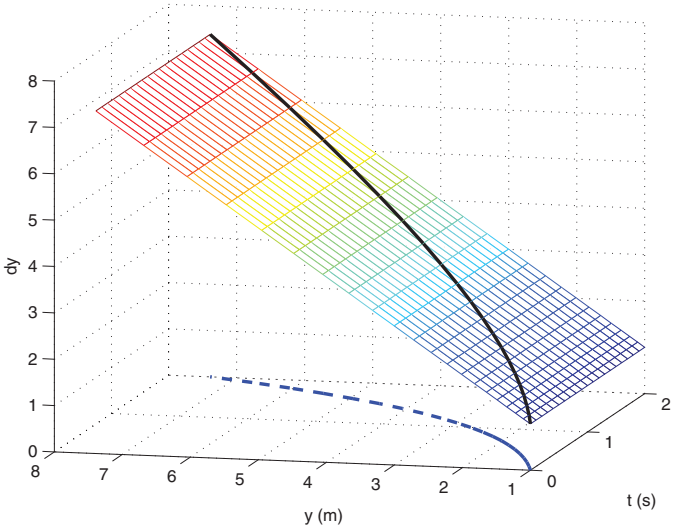

Fig. 1. 3D surface visualization for the differential jet space of Eq. (6) including the solution curve (blue dashed lines) and prolonged solution space curve (black solid lines).(For interpretation of the references to color in this figure legend, the reader is referred to the web version of this article.)

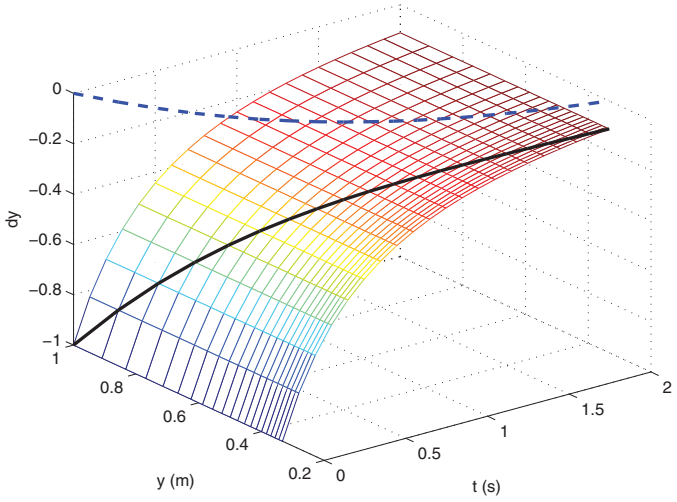

Fig. 2. 3D surface visualization for the differential jet space of Eq. (7) including the solution curve (blue dashed lines) and prolonged solution space curve (black solid lines). (For interpretation of the references to color in this figure legend, the reader is referred to the web version of this article.)

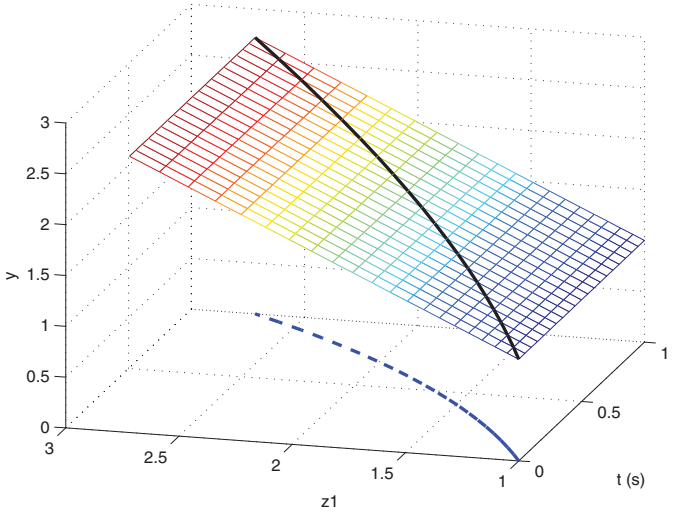

Fig. 3. 3D surface visualization for the potential jet space of Eq. (12) including the solution curve (blue dashed line) and prolonged solution space curve (black solid line). (For interpretation of the references to color in this figure legend, the reader is referred to the web version of this article.)

$\mathbb{R}$. Therefore, the solution space on the (t, y) plane can be considered as a projection of the differential jet space onto the plane. The major advantage of differential jet spaces is that significant information is available on the solution space without having to explicitly solve the differential equations. A common application to this concept is symmetries of (partial) differential equations.

2.2. Potential jet space

2.2.1. Definition

Definition 3. The **monomial potential** $V^{i,j}$ of order k is given by [23]:

$$V_t^{i,j} = t^i y^j,$$

where $j \neq 0$ and $i + j = k$.

Define

$$\frac{dz}{dt} = V^{0,1}, \quad \frac{dv}{dt} = V^{1,1}, \quad \frac{dw}{dt} = V^{0,2}. \tag{10}$$

Thus, z is an order 1 monomial potential and v, w are order 2 monomial potentials. Hence there are $K = \frac{k(k+1)}{2}$ order k monomial potentials,

$$V_t^{k-1,1} = t^{k-1} y, \quad V_t^{k-2,2} = t^{k-2} y^2, \ldots, \quad V_t^{0,k} = y^k.$$

and for a given curve $y = y(t)$,

$$z = \int_0^t y \, dt, \quad v = \int_0^t ty \, dt, \quad w = \int_0^t y^2 \, dt \tag{11}$$

Definition 4. The **potential jet space** J_p^n, $n \geq 1$ is the Euclidean space $\mathbb{R}^{n+2}$ with local coordinates $(t, y, V_{(n)})$ where $V_{(n)}$ consists of monomial potentials up to the kth order (where k is the largest integer such that $K \leq n$) plus (if $n \neq K$) the potentials

$$V^{k,1}, \ V^{k-1,2}, \ldots, \ V^{k-(n-K)+1,n-K}$$

For example,

$$J_p^1 = (t, y, V^{0,1}) \approx \mathbf{R}^3$$
$$J_p^2 = (t, y, V^{0,1}, V^{1,1}) \approx \mathbf{R}^4$$
$$J_p^3 = (t, y, V^{0,1}, V^{1,1}, V^{0,2}) \approx \mathbf{R}^5$$

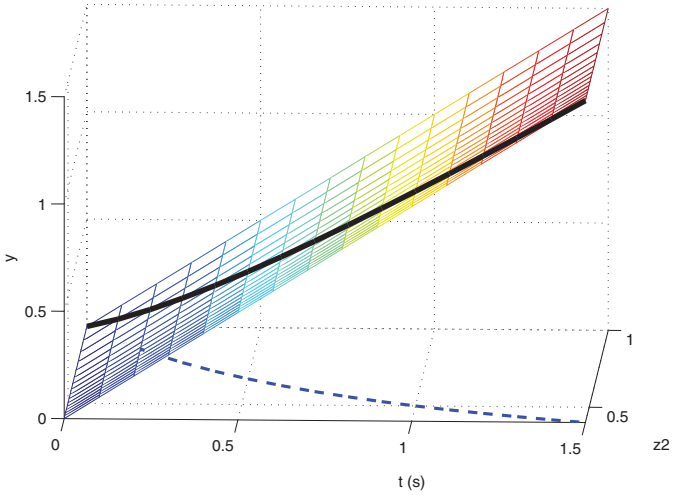

Fig. 4. 3D surface visualization for the potential jet space of Eq. (13) including the solution curve (blue dashed line) and prolonged solution space curve (black solid line). (For interpretation of the references to color in this figure legend, the reader is referred to the web version of this article.)

2.2.2. Geometric interpretation of the potential jet space

To investigate the geometric aspects of the potential jet space, a similar analysis to Section 2.1.1 is used for the first order differential equations (6) and (7). Integrating Eqs. (6) and (7) from 0 to t and writing in terms of potentials yields:

$$y - z_1 = y_0, \quad y_0 = 1 \tag{12}$$
$$y + z_2 = y_0, \quad y_0 = 1 \tag{13}$$

where:

$$\frac{dz_1}{dt} = y, \quad \frac{dz_2}{dt} = y^2 \tag{14}$$

The potential jet space surfaces of Eqs. (12) and (13), the solutions of Eqs. (8) and(9) and their prolongations onto the potential jet space are plotted in Figs. 3 and 4. Notice that the potential jet space of Fig. 4 is a linear plane even though the underlying model of Eq. (7) is nonlinear. Furthermore, the prolongation of a measured curve $(t, y(t))$ onto the potential jet space surface involves integrals so is robust to noise since an integral is a bounded operator that attenuates noise.

On the other hand derivatives are unbounded operators that amplify noise.

2.3. Identifiability of linear systems

An input–output map $(\mathbf{p}, u(t)) \mapsto \Sigma_{\mathbf{x}_0}(\mathbf{p}, u)$ of the state-space equation describing the dynamics of a single-input, single output, linear compartmental model, for a given input and initial state, is defined as:

$$\dot{\mathbf{x}} = \mathbf{A}(\mathbf{p})\mathbf{x} + \mathbf{b}\,u(t) \tag{15}$$

$$y = \mathbf{M}\mathbf{x}$$

$$\mathbf{x} \equiv [x_1, x_2, \ldots, x_n]^T,\ \mathbf{x}(0) \equiv \mathbf{x}_0 = [x_{10}, x_{20}, \ldots, x_{n0}]^T,$$

$$y \equiv y(t) = x_1,\ \mathbf{M} \equiv [1, 0, \ldots, 0]^T \tag{16}$$

$$\mathbf{p} = [p_1, p_2, \ldots, p_n]^T,\ \mathbf{b} \equiv [b_1, 0, \ldots, 0]^T \tag{17}$$

where $x_i = x_i(t), i = 1, \ldots, n$ is a quantity in compartment i at time $t(s)$, $\mathbf{x}$ an $n \times 1$ state vector, $\mathbf{x_0}$ the initial condition of state $\mathbf{x}$, y the measured compartment, u the input, $\mathbf{A}(\mathbf{p})$ an $n \times n$ matrix, $\mathbf{b}$ an $n \times 1$ matrix, $\mathbf{p}$ a vector of parameters representing the transfer rates between compartments, and $\mathbf{C}$ a $1 \times n$ matrix. The assumption is that the input u is a free variable, and does not depend on $\mathbf{x}_0$.

Global or structural identifiability characterizes a unique set of model parameters that describes the observed dynamics in the absence of noise [41]. Given arbitrary sets of parameter vectors $\mathbf{p_1}$ and $\mathbf{p_2}$, with $\mathbf{p_1} \neq \mathbf{p_2}$, and assuming that both sets of vectors of the systems $\Sigma_{\mathbf{x}_0}(\mathbf{p_1}, u)$ and $\Sigma_{\mathbf{x}_0}(\mathbf{p_2}, u)$ described in Eq. (15) are excited at the same initial state, three possible scenarios occur [41]:

1. The system is termed structurally globally or uniquely identifiable if, for a parameter vector $\mathbf{p} \in \mathbb{R}^n$,
$$\Sigma_{\mathbf{x}_0}(\mathbf{p_1}, u) = \Sigma_{\mathbf{x}_0}(\mathbf{p_2}, u) \implies \mathbf{p_1} = \mathbf{p_2} \tag{18}$$
2. The system is termed locally identifiable if, for a parameter vector $\mathbf{p} \in \mathbf{P}$, there is a neighborhood $\mathbf{V_p}$ such that
$$\mathbf{p_1}, \mathbf{p_2} \in \mathbf{V_p} \text{ and } \Sigma_{\mathbf{x}_0}(\mathbf{p_1}, u) = \Sigma_{\mathbf{x}_0}(\mathbf{p_2}, u) \implies \mathbf{p_1} = \mathbf{p_2} \tag{19}$$
3. The system is termed unidentifiable if, for a parameter vector $\mathbf{p} \in \mathbf{P}$, there is no neighborhood $\mathbf{V_p}$ such that Eq. (19) holds:
$$\forall \mathbf{V_p},\ \exists \mathbf{p_1}, \mathbf{p_2} \in \mathbf{V_p},\ \text{where } \mathbf{p_1} \neq \mathbf{p_2} \text{ and } \Sigma_{\mathbf{x}_0}(\mathbf{p_1}, u) = \Sigma_{\mathbf{x}_0}(\mathbf{p_2}, u) \tag{20}$$

2.4. Differential jet space approach to identifiability

A common approach to analyze identifiability of compartmental systems is the differential jet space approach of Ljung and Glad [28]. This approach has been implemented in a DAISY (Differential Algebra for Identifiability of SYstems) program [10].

This method constructs an input–output map in an implicit form using a process called Ritt's pseudodivision algorithm [10]. The output of this process is a characteristic set, which is a finite "minimal" set of the differential polynomial that would generate the same differential ideals as the original system of Eq. (15) (see Ref. [10]). The equations of the characteristic set do not contain the state variables, and are hence termed input–output relations, which can be described by:

$$\theta(\mathbf{y}, \dot{\mathbf{y}}, \ldots, \mathbf{u}, \dot{\mathbf{u}}, \ldots, \mathbf{p}) = \mathbf{0} \tag{21}$$

Note that Eq. (21) are polynomial equations in $\mathbf{u}, \dot{\mathbf{u}}, \ldots, \mathbf{y}, \dot{\mathbf{y}}, \ldots$ called differential polynomials, with rational coefficients in the parameter $\mathbf{p}$. Structural identifiability can be determined by testing coefficients $\mathbf{c}(\mathbf{p})$ of the input–output model in terms of the criteria in Eq. (18). This test constructs a map called an exhaustive summary of the system. The exhaustive summary normally admits a system of nonlinear equations which may be solved using a suitable algebraic method such as the Buchberger algorithm [12]. This algorithm constructs a Groebner basis, whose structure makes it possible to see whether the nonlinear equation system admits one solution, infinitely many solutions, or no solutions. Thus, it can be determined if the system is uniquely identifiable, locally identifiable, or structurally unidentifiable.

In terms of visualizing the differential jet space as introduced in Section 2.1.1, the input–output differential equation is a multidimensional jet space surface that is characterized by coordinates that are all measurable. Hence, in principle, the jet space surface of the input–output differential equation will admit all the derivatives of the measured data in the absence of noise. Hence the unknown coefficients of the jet-space coordinates can be uniquely characterized from this space curve. However, in practice differentiating data is too noisy so this approach is not practically feasible.

2.4.1. Linear algebra method for obtaining the input–output equations from linear compartmental models

Note that for the analysis of identifiability, the use of Ritt's pseudodivision algorithm is computationally intense. To simplify computations and to provide a method that can be extended to the potential jet space, a simpler linear algebra approach, tailored to linear compartmental models is developed.

Eq. (15) is differentiated $n-1$ times which yields n matrix equations:

$$\dot{\mathbf{x}} = \mathbf{A}\mathbf{x} + \mathbf{b}\,u(t) \tag{22}$$

$$\mathbf{x}^{(i+1)} = \mathbf{A}\mathbf{x}^{(i)} + \mathbf{b}\,u^{(i)}(t), \quad i = 1, \ldots, n-1 \tag{23}$$

where $\mathbf{x}^{(i)}$ denotes the ith derivative of the states vector $\mathbf{x}$, and $u^{(i)}(t)$ denotes the ith derivative of the input.

After separating out the $x_1, \ldots, x_1^{(n)}$ equations, the system of Eqs. (22) and (23) can be written in the form:

$$\begin{aligned} \dot{x}_1 &= A_{11}x_1 + A_{12}x_2 + \cdots + A_{1n}x_n + b_1 u(t) \\ \ddot{x}_1 &= A_{11}\dot{x}_1 + A_{12}\dot{x}_2 + \cdots + A_{1n}\dot{x}_n + b_1 \dot{u}(t) \end{aligned} \tag{24a}$$

$$\vdots$$

$$x_1^{(n)} = A_{11}x_1^{(n-1)} + A_{12}x_2^{(n-1)} + \cdots + A_{1n}x_n^{(n-1)} + b_1 u^{(n-1)}(t) \tag{24b}$$

$$\begin{aligned} \dot{\bar{\mathbf{x}}} &= \mathbf{C}_{\mathbf{1},\bar{\mathbf{A}}}\, x_1 + \bar{\mathbf{A}}\,\bar{\mathbf{x}} \\ &\vdots \\ \bar{\mathbf{x}}^{(n)} &= \mathbf{C}_{\mathbf{1},\bar{\mathbf{A}}}\, x_1^{(n-1)} + \bar{\mathbf{A}}\,\bar{\mathbf{x}}^{(n-1)} \end{aligned} \tag{25}$$

where:

$$\bar{\mathbf{A}} = \begin{bmatrix} A_{22} & A_{23} & \ldots & A_{2n} \\ A_{32} & A_{33} & \ldots & A_{3n} \\ \vdots & \vdots & \ddots & \vdots \\ A_{n2} & A_{n3} & \ldots & A_{nn} \end{bmatrix}, \qquad \mathbf{C}_{\mathbf{1},\bar{\mathbf{A}}} = [A_{21}, A_{31}, \ldots, A_{n1}]^T \tag{26}$$

$$\bar{\mathbf{x}} = [x_2, \ldots, x_n]^T \tag{27}$$

$$\text{Known states} \equiv x_1, \dot{x}_1, \ldots, x_1^{(n)} \tag{28}$$

$$\text{Unknown states} \equiv \bar{\mathbf{x}}, \dot{\bar{\mathbf{x}}}, \ldots, \bar{\mathbf{x}}^{(n)} \tag{29}$$

Eqs. (25) are now written in the form:

$$-\Phi\bar{\mathbf{X}} = \begin{bmatrix} \mathbf{C}_{\mathbf{1},\bar{\mathbf{A}}}x_1 \\ \vdots \\ \mathbf{C}_{\mathbf{1},\bar{\mathbf{A}}}x_1^{(n-1)} \end{bmatrix} \tag{30}$$

where:

$$\Phi = \begin{bmatrix} \bar{\mathbf{A}} & -\mathbf{I}_{n-1} & \mathbf{0}_{n-1} & \dots & \mathbf{0}_{n-1} \\ \mathbf{0}_{n-1} & \bar{\mathbf{A}} & -\mathbf{I}_{n-1} & \dots & \mathbf{0}_{n-1} \\ \vdots & \vdots & \ddots & \ddots & \vdots \\ \mathbf{0}_{n-1} & \mathbf{0}_{n-1} & \mathbf{0}_{n-1} & \bar{\mathbf{A}} & -\mathbf{I}_{n-1} \end{bmatrix} \equiv n(n-1) \times n^2 - 1 \text{ matrix} \tag{31}$$

$$\begin{aligned} &\mathbf{0}_{n-1} \equiv n-1 \times n-1 \text{ matrix of zeros,} \\ &\mathbf{I}_{n-1} \equiv (n-1) \times (n-1) \text{ identity matrix} \end{aligned} \tag{32}$$

$$\overline{\mathbf{X}} = \begin{bmatrix} \overline{\mathbf{x}} \\ \overline{\mathbf{x}}^{(1)} \\ \vdots \\ \overline{\mathbf{x}}^{(n)} \end{bmatrix} \equiv (n^2-1) \times 1 \text{ vector} \tag{33}$$

Adding the $n-1$ equations given in Eq. (24b) to the matrix system of Eqs. (30)–(33) yields:

$$\mathbf{M}\,\overline{\mathbf{X}} = \mathbf{B} \tag{34}$$

$$\mathbf{M} = \begin{bmatrix} \mathbf{0_{n-1}} \mathbf{D}_{\mathbf{R}_{1,\bar{\mathbf{A}}}} \mathbf{0_{n-1}} \\ \hline -\Phi \end{bmatrix} \equiv (n^2-1) \times (n^2-1) \text{ matrix} \tag{35}$$

$$\mathbf{B} = \begin{bmatrix} \ddot{x}_1 - A_{11}\dot{x}_1 - b_1 u(t) \\ \vdots \\ x_1^{(n)} - A_{11} x_1^{(n-1)} - b_1 u^{(n-1)}(t) \\ \mathbf{C}_{\mathbf{1},\bar{\mathbf{A}}}\, x_1 \\ \vdots \\ \mathbf{C}_{\mathbf{1},\bar{\mathbf{A}}}\, x_1^{(n-1)} \end{bmatrix} \equiv (n^2-1) \times 1 \text{ vector} \tag{36}$$

where:

$$\mathbf{D}_{\mathbf{R}_{1,\bar{\mathbf{A}}}} = \begin{bmatrix} \mathbf{R}_{1,\bar{\mathbf{A}}} & \mathbf{0}_{1\times n-1} & \dots & \mathbf{0}_{1\times n-1} \\ \mathbf{0}_{1\times n-1} & \mathbf{R}_{1,\bar{\mathbf{A}}} & \dots & \mathbf{0}_{1\times n-1} \\ \vdots & \vdots & \ddots & \vdots \\ \mathbf{0}_{1\times n-1} & \mathbf{0}_{1\times n-1} & \dots & \mathbf{R}_{1,\bar{\mathbf{A}}} \end{bmatrix} \equiv n-1 \times n-1 \text{ matrix} \tag{37}$$

$$\mathbf{R}_{1,\bar{\mathbf{A}}} = [A_{12}, \cdots, A_{1n}], \quad \mathbf{0}_{1\times n-1} \equiv 1 \times n-1 \text{ matrix of zeros} \tag{38}$$

Eq. (34) represents n^2-1 equations in the n^2-1 unknowns of Eq. (29). The parameters $x_2, \dots, x_n$ from solution $\overline{\mathbf{X}}$ of Eq. (34) are substituted into Eq. (24a) to yield the input–output equation which corresponds to exhaustive summary. For future reference, Eq. (24a) is referred to as the "substitution equation".

Note that even in the case of a non-unity observational gain in Eq. (16) the final substitution equation will still be written directly in terms of the measured data. Since the methods in this paper operate on the substitution equation, a non-unity observational gain will have no effect on the overall global identifiability theory and implementation. Hence, for simplicity in demonstrating the methods, it is assumed without loss of generality that the observational gain is 1. Also note that this paper looks at the most difficult case where unknown parameters are present in compartments that are not measured and there is only one known state with all the remaining states unknown. Multiple measured compartments would significantly reduce the order and complexity of the final input–output equations since there would be fewer unknown states. Therefore, this case is not considered as well.

2.4.2. Example: two compartmental model

Consider a state space model of a two compartment system defined:

$$\begin{aligned} \dot{\mathbf{x}} &= \begin{bmatrix} -a_1 & a_2 \\ -a_3 & a_4 \end{bmatrix} \mathbf{x} + \begin{bmatrix} 1 \\ 0 \end{bmatrix} u(t) \\ y(t) &= [1\ 0]\,\mathbf{x} \end{aligned} \tag{39}$$

For the system $n=2$, the substitution equation is:

$$\dot{x}_1 = -a_1 x_1 + a_2 x_2 + b_1 u(t) \tag{40}$$

The system of equations is given by:

$$\mathbf{M}\,\overline{\mathbf{X}} = \mathbf{B} \tag{41}$$

where:

$$\mathbf{M} = \begin{bmatrix} 0 & a_2 & 0 \\ a_4 & -1 & 0 \\ 0 & 0 & -1 \end{bmatrix}, \quad \mathbf{B} = \begin{bmatrix} \ddot{x}_1 + a_1\dot{x} - \ddot{u} \\ a_3 x_1 \\ a_3 \dot{x}_1 \end{bmatrix}, \quad \overline{\mathbf{X}} = \begin{bmatrix} x_2 \\ \dot{x}_2 \\ \ddot{x}_2 \end{bmatrix} \tag{42}$$

Solving Eqs. (41) and (42) yields the unknown states $\overline{\mathbf{X}}$ and thus the unknown states $\overline{\mathbf{x}}$ in Eq. (29) with $n=2$. These unknown states are substituted into Eq. (40) to give the following input–output equation:

$$\ddot{x}_1 + (a_1 - a_4)\dot{x}_1 + (a_2 a_3 - a_1 a_4) x_1 + a_4 u - \dot{u} = 0 \tag{43}$$

To construct the exhaustive summary of the differential input–output equation of Eq. (43), the coefficients of the input–output polynomial are extracted:

$$a_1 - a_4, \quad a_2 a_3 - a_1 a_4, \quad a_4 \tag{44}$$

Following the method of [10], the coefficients in Eq. (44) are evaluated at a symbolic parameter value $\mathbf{p} = [\alpha_1, \alpha_2, \alpha_3]$ to determine the range of the input–output function. The result is the following set of algebraic nonlinear equations:

$$a_1 - a_4 = \alpha_1, \quad a_2 a_3 - a_1 a_4 = \alpha_2, \quad a_4 = \alpha_3 \tag{45}$$

Using the Buchberger algorithm, the solution to the non-linear system of Eq. (45) is:

$$\begin{aligned} a_1 &= \alpha_2 + \alpha_3 \\ a_2 &= \frac{\alpha_2 + (\alpha_2 + \alpha_3)\alpha_3}{a_3} \\ a_3 &= s \\ a_4 &= \alpha_3 \end{aligned} \tag{46}$$

where s is an arbitrary parameter so there are infinitely many solutions to the non-linear system of Eq. (45). In other words, for any constant $a_3 = s$, the input–output relationship of Eq. (43) has the same solution y_1, so the system model is unidentifiable.

Note that the linear algebra method presented is a prolongation of the original differential equation onto the second order differential jet space to eliminate the unobserved state x_2. Furthermore, since the formulation involves high order derivatives, it is not practical to use this method to identify the parameters in the presence of measurement errors.

2.5. Potential jet space approach

2.5.1. Obtaining the input–output equation for linear systems

To compute the potential input–output equation, a linear algebra method similar to the differential input–output equation is implemented. The monomials in this method are the monomial potentials defined in Definition 3. Denote the following integral operator:

$$I^{(k)} X = \underbrace{\int_0^t \dots \int_0^t}_{k \text{ times}} X \, \mathrm{d}t \dots \mathrm{d}t \tag{47}$$

Theorem 5. *The operator of Eq. (47) on an arbitrary function $F(t)$ can be written as the sum of the monomial potentials of Definition 3:*

$$I^{(n)}(F(t)) = \frac{1}{(n-1)!}\sum_{k=1}^{n}\binom{n-1}{k-1}(-1)^{k+1}t^{n-k}V^{k-1,1} \tag{48}$$

where $\binom{n}{k}$ is the binomial coefficient indexed by n and k, and $\frac{d}{dt}V^{k-1,1} = t^{k-1}F(t)$

Proof. See proof of Theorem 5 in Appendix A. □

Theorem 5 implies that the n successive integrations of $y(t)$ with the respect to time t (of any order) can be replaced with the sum of single integrals with respect to time (from integration by parts as shown in the proof). In terms of potential jet space prolongation, this is equivalent to prolonging $y(t)$ onto the potential jet space with co-ordinates:

$$(t, x, t_0, x_0, V^{0,1}, V^{1,1}, \ldots, V^{n-1,1}) \tag{49}$$

To compute the potential input–output equation, the integral operator of Eq. (47) is operated on the system Eq. (15) $2n-1$ times to yield a total of $2n-1$ matrix equations:

$$I^{(i-1)}\mathbf{x} - \frac{t^{i-1}}{(n-1)!}\mathbf{x_0} = \mathbf{A}\,I^{(i)}\mathbf{x} + \mathbf{b}\,I^{(i)}u(t), \quad i = 1, \ldots, 2n-1 \tag{50}$$

where:

$$\text{known (measured) data} = x_1, \tag{51}$$

$$\text{unknown states} \equiv \mathbf{x_0}, \overline{\mathbf{x}}, I^{(1)}\,\overline{\mathbf{x}}, \ldots, I^{(2n-1)}\,\overline{\mathbf{x}} \tag{52}$$

$$\overline{\mathbf{x}} = [x_2, \ldots, x_n]^T \tag{53}$$

$$\mathbf{x_0} \equiv \text{ Initial condition} \tag{54}$$

To make the formulation as general as possible, the values of the initial condition vector defined in Eq. (54) are also treated as unknowns. Eqs. (50)–(54) describe a total of $n(2n-1)$ equations in $n(2n-1)$ unknown states, as described in Eq. (52).

Eq. (50) is written in the form:

$$\begin{aligned}
x_1 - x_{1,0} &= \mathbf{A}_{11}I^{(1)}x_1 + \mathbf{A}_{1,(2\ldots n)}I^{(1)}\overline{\mathbf{x}} + b_1I^{(1)}u(t)\\
x_2 - x_{2,0} &= \mathbf{A}_{21}I^{(1)}x_1 + \mathbf{A}_{2,(2\ldots n)}I^{(1)}\overline{\mathbf{x}}\\
&\vdots\\
x_n - x_{n,0} &= \mathbf{A}_{n1}I^{(1)}x_1\mathbf{A}_{n,(2\ldots n)}I^{(1)}\overline{\mathbf{x}}\\
I^{(1)}x_1 - t\,x_{1,0} &= \mathbf{A}_{11}I^{(2)}x_1 + \mathbf{A}_{1,(2\ldots n)}I^{(2)}\overline{\mathbf{x}} + b_1I^{(1)}u(t)\\
&\vdots\\
I^{(1)}x_n - t\,x_{n,0} &= \mathbf{A}_{n1}I^{(2)}x_1 + \mathbf{A}_{n,(2\ldots n)}I^{(2)}\overline{\mathbf{x}}\\
&\vdots\\
I^{(2n-2)}x_1 - \frac{t^{2n-2}}{(2n-2)!}\,x_{1,0} &= \mathbf{A}_{11}I^{(2n-1)}x_1\\
&\quad + \mathbf{A}_{1,(2\ldots n)}I^{(2n-1)}\overline{\mathbf{x}} + b_1I^{(2n-1)}u(t)\\
&\vdots\\
I^{(2n-2)}x_n - \frac{t^{2n-2}}{(2n-2)!}\,x_{n,0} &= \mathbf{A}_{n1}I^{(2n-1)}x_1 + \mathbf{A}_{n,(2\ldots n)}I^{(2n-1)}\overline{\mathbf{x}}
\end{aligned} \tag{55, 56}$$

where $\mathbf{A}_{i,(2\ldots n)}$ denotes a vector whose elements are the second column to the nth column, for a fixed ith row, $i = 1, \ldots, n$.
For future reference, Eq. (55) is referred to as the "substitution equation". Eq. (56) is used to solve for the unknown states of Eq. (52), in terms of the known states defined by:

$$\text{known states} \equiv x_1, I^{(1)}x_1, \ldots, I^{(2n-1)}x_1 \tag{57}$$

Eq. (56) is now written in the augmented matrix form:

$$\mathbf{M}\,\overline{\mathbf{X}} = \mathbf{B} \tag{58}$$

where:

$$\mathbf{M} = \begin{bmatrix}
\mathbf{I}_n & \mathbf{D_2} & \overline{\mathbf{A}} & \mathbf{0}_{n\times(n-1)} & \cdots & \mathbf{0}_{n\times(n-1)}\\
t\,\mathbf{I}_n & \mathbf{0}_{n\times(n-1)} & \mathbf{D_2} & \overline{\mathbf{A}} & \cdots & \mathbf{0}_{n\times(n-1)}\\
\vdots & \vdots & \vdots & \ddots & \ddots & \vdots\\
\dfrac{t^{2n-2}}{(2n-1)!}\,\mathbf{I}_n & \mathbf{0}_{n\times(n-1)} & \mathbf{0}_{n\times(n-1)} & \cdots & \mathbf{D_2} & \overline{\mathbf{A}}
\end{bmatrix} \tag{59}$$

$$\equiv 2n^2 - n \times 2n^2 - n \text{ matrix}$$

$$\overline{\mathbf{X}} = \begin{bmatrix}
\mathbf{x_0}\\
\overline{\mathbf{x}}\\
I^{(1)}\,\overline{\mathbf{x}}\\
\vdots\\
I^{(2n-1)}\,\overline{\mathbf{x}}
\end{bmatrix} \equiv 2n^2 - n \times 1 \text{ vector} \tag{60}$$

$$\mathbf{B} = \begin{bmatrix}
x_1 - A_{11}I^{(1)}x_1 - b_1I^{(1)}u(t)\\
-\mathbf{A}_{2\ldots n,1}I^{(1)}x_1\\
\vdots\\
I^{(2n-2)}x_1 - A_{11}I^{(2n-1)}x_1 - b_1I^{(2n-1)}u(t)\\
-\mathbf{A}_{2\ldots n,1}I^{(2n-1)}x_1
\end{bmatrix} \equiv 2n^2 - n \times 1 \text{ vector} \tag{61}$$

$$\mathbf{D_2} = \begin{bmatrix}\mathbf{0}_{1\times n-1}\\ \hline \mathbf{I}_{n-1}\end{bmatrix}, \quad \mathbf{0}_{n-1} \text{ and } \mathbf{I}_{n-1} \equiv \text{Eq.(32)} \tag{62}$$

$$\text{and } \overline{\mathbf{A}} \equiv \text{ Eq (26)} \tag{63}$$

The solution to the augmented matrix equation (58) is then substituted into Eq. (55) to yield the potential input–output equation. The coefficients of the potential terms from this input–output equation are then extracted and are called the potential exhaustive summary, which represents a map of the system onto the potential jet space.

2.5.2. Example: two compartment model

To further clarify the potential exhaustive summary, consider the two compartmental model of Eq. (39). Applying Eqs. (59)–(63), the potential augmented matrices are:

$$\mathbf{M} = \begin{bmatrix}
1 & 0 & 0 & a_2 & 0 & 0\\
0 & 1 & -1 & a_4 & 0 & 0\\
t & 0 & 0 & 0 & a_2 & 0\\
0 & t & 0 & -1 & a_4 & 0\\
\frac{t^2}{2} & 0 & 0 & 0 & 0 & a_2\\
0 & \frac{t^2}{2} & 0 & 0 & -1 & a_4
\end{bmatrix} \tag{64}$$

$$\overline{\mathbf{X}} = \begin{bmatrix}
\mathbf{x_0}\\
x_2\\
I^{(1)}\,x_2\\
I^{(2)}\,x_2\\
I^{(3)}\,x_2
\end{bmatrix}, \quad \mathbf{B} = \begin{bmatrix}
x_1 + a_1I^{(1)}x_1 - b_1I^{(1)}u(t)\\
a_3I^{(1)}x_1\\
I^{(1)}x_1 + a_1I^{(2)}x_1 - b_1I^{(2)}u(t)\\
a_3I^{(2)}x_1\\
I^{(2)}x_1 + a_1I^{(3)}x_1 - b_1I^{(3)}u(t)\\
a_3I^{(3)}x_1
\end{bmatrix}, \tag{65}$$

where $\mathbf{x_0}$ is defined in Eq. (54).

Solving Eq. (58) using the matrices in Eq. (65), and substituting the resulting solution for the potential of the unknown state $I^{(1)}\,\mathbf{x_u}$ give, after simplifying in Maple, the following input–output equation:

$$x_1 - x_{1,0} - \dot{x}_{1,0}\,t + (a_1 - a_4)\int_0^t x_1\,\mathrm{d}t - (a_1 - a_4)y_0\,t + (a_2a_3 - a_1a_4)\int_0^t\int_0^t x_1\,\mathrm{d}t\mathrm{d}t + a_4\int_0^t\int_0^t u\,\mathrm{d}t\mathrm{d}t - \int_0^t u\,\mathrm{d}t - u_0\,t = 0 \tag{66}$$

Setting $y(t) \equiv x_1(t)$ gives the final integral input–output equation:

$$y(t) - y_0 - (dy_0 + u_0)\,t + (a_1 - a_4)\int_0^t y\,\mathrm{d}t - (a_1 - a_4)y_0\,t + (a_2a_3 - a_1a_4)\int_0^t\int_0^t y\,\mathrm{d}t\mathrm{d}t + a_4\int_0^t\int_0^t u\,\mathrm{d}t\mathrm{d}t - \int_0^t u\,\mathrm{d}t = 0 \tag{67}$$

where y_0 denotes the amount of measured quantity at $t = 0$, and dy_0 denotes the derivative initial condition. The potential exhaustive summary is derived from Eq. (67) in exactly the same way as was done for Eqs. (43) and (44). That is, the unknown coefficients in front of the terms involving the independent known polynomial variables, are extracted. These terms are $\int_0^t y\mathrm{d}t$, $y_0\,t$, $\int_0^t\int_0^t y\,\mathrm{d}t$, $\int_0^t\int_0^t u\,\mathrm{d}t$. However, note that Eq. (67) can be written in the form:

$$y(t) - y_0 - (dy_0 + u_0)\,t + (a_1 - a_4)\int_0^t (y - y_0)\,\mathrm{d}t + (a_2a_3 - a_1a_4)\int_0^t\int_0^t y\,\mathrm{d}t\mathrm{d}t + a_4\int_0^t\int_0^t u\,\mathrm{d}t\mathrm{d}t - \int_0^t u\,\mathrm{d}t = 0 \tag{68}$$

Hence, the extra coefficients of y_0 and dy_0 do not provide any further independent combinations of unknown parameters for the exhaustive summary. In other words, the initial conditions can be ignored in the exhaustive summary. The resulting coefficients of the input–output polynomial are:

$$a_1 - a_4, \quad a_2a_3 - a_1a_4, \quad a_4 \tag{69}$$

Eq. (69) is the same as Eq. (44) for the differential jet space. Alternatively, taking the integral operator $I^{(n)}(X)$ on the differential input–output equation of Eq. (43) yields the identical result. Hence there is a one-to-one relationship between the differential and potential jet space approaches. Replacing $\int_0^t\int_0^t x_1\,dt\,dt$ by $t\int_0^t x_1\,dt - \int_0^t tx_1\,dt$ (integration by parts) shows that Eq. (66) is equivalent to the prolongation of the original state space system described by Eq. (39) onto the potential jet space with co-ordinates:

$$J_p^2 \equiv t, x_1, z_1, z_2 \tag{70}$$

$$\frac{dz_1}{dt} = x_1, \quad \frac{dz_2}{dt} = tx_1. \tag{71}$$

The final part of the algorithm follows the same procedure as Eqs. (45) and (46) to prove global identifiability.

2.5.3. Parameter identification—two compartment model

Eq. (67) has a major advantage over Eq. (43) in that it involves integrals instead of differentials. Thus, the noisy data $y(t)$ can be substituted into Eq. (67) to enable parameter identification of the unknown parameters $a_1, \ldots a_4$, which is not possible using Eq. (43), since the derivative is an unbounded operator that amplifies noise. On the other hand, the integral operator is a bounded operator that reduces noise. Note that the trapezium rule is used to compute all integrals in this paper.

Set $y_{\mathrm{model}}(t) = y_{\mathrm{meas}}(t)$ in Eq. (67) and put $a_3 = 1$ to allow for identifiability as proven in Eqs. (44)–(46). Substitute N values of $t \in \{t_1, \ldots, t_N\}$ into the right hand side of Eq. (67) to yield a set of N equations in 5 unknowns. The resulting set of integral equations can be written in the form:

$$\mathbf{M_{p\text{-}jet}}\,\mathbf{p} = \mathbf{b_{p\text{-}jet}} \tag{72}$$

$$\mathbf{M_{p-jet}} = \left[\mathbf{1_{N\times 1}}|\mathbf{T_{N\times 1}}|I^{(1)}\mathbf{y}_{N\times 1}|I^{(2)}\mathbf{y}_{N\times 1}|I^{(2)}\mathbf{u}_{N\times 1}\right] \equiv \text{coefficients from potential jet space formulation} \tag{73}$$

$$\mathbf{1_{N\times 1}} \equiv N\times 1 \text{ number of ones}, \quad \mathbf{T_{N\times 1}} \equiv \begin{bmatrix} t(1) \\ \vdots \\ t(N) \end{bmatrix} \tag{74}$$

$$\mathbf{b_{p-jet}} = \begin{bmatrix} y_{\mathrm{meas}}(t_1) - \int_0^{t_1} u\,\mathrm{d}t \\ \vdots \\ y_{\mathrm{meas}}(t_N) - \int_0^{t_N} u\,\mathrm{d}t \end{bmatrix}, \quad \mathbf{p} = \begin{bmatrix} y0 \\ dy_{0b} \\ \alpha_1 \\ \alpha_2 \\ \alpha_3 \end{bmatrix} \tag{75}$$

$$dy_{0b} = dy_0 + (a_1 - a_4)y_0 + u_0, \quad \alpha_1 = a_1 - a_4 \quad \alpha_2 = a_1a_4 - a_2a_3, \quad \alpha_3 = a_4 \tag{76}$$

$$I^{(i)}\,\mathbf{W_{N\times 1}} \equiv \begin{bmatrix} I^{(i)}W(t_1) \\ \vdots \\ I^{(i)}W(t_N) \end{bmatrix}, \mathbf{W} = \mathbf{y_{N\times 1}} \text{ or } \mathbf{u_{N\times 1}},\ i = 1, 2,$$

$I^{(i)}(X)$ is the integral operator of Eq.(47). (77)

Eq. (72) is solved by linear least squares, which determines the best fit of the right hand side of Eq. (67) to the measured data. The required unknown parameters $\{y_0, dy_0, a_1, a_2, a_4\}$ are determined by solving Eq. (76) by the Buchberger algorithm.

Hence, the potential jet space global identifiability theory can be used in practice to directly identify the model in presence of noise and modeling error without requiring any solution to the model differential equations. This feature is in contrast to the conventional differential jet space identifiability theory, which requires computation of high order derivatives and other methods like Raue *et al.* [35] which require numerical solutions of the model. The method can also be used to do standard statistical sensitivity analysis to ensure there are no parameters that are theoretically identifiable but in practice have such a small effect on the model output response that they are effectively unidentifiable.

The algorithm for identifying a dynamical model using the potential jet space identifiability theory is summarized in Fig. 5.

2.6. Special case—first order glucose–insulin model

Consider a simplified model describing the dynamics of glucose–insulin which has been applied extensively in critical care [22]:

$$\dot{G} = -p_G G - S_I\,(G + G_E)\,\overline{Q} + P(t) \tag{78}$$

$$\overline{Q}(t) = \frac{Q}{1 + \alpha_G Q} \tag{79}$$

where $G(t)$ is the concentration of plasma glucose above the equilibrium level (mmol/L); G_E the equilibrium level of plasma glucose concentration (mmol/L); $Q(t)$ the interstitial insulin level (mU/L); $P(t)$ the exogenous glucose infusion rate (mmol/(L min)); $u(t)$ the insulin

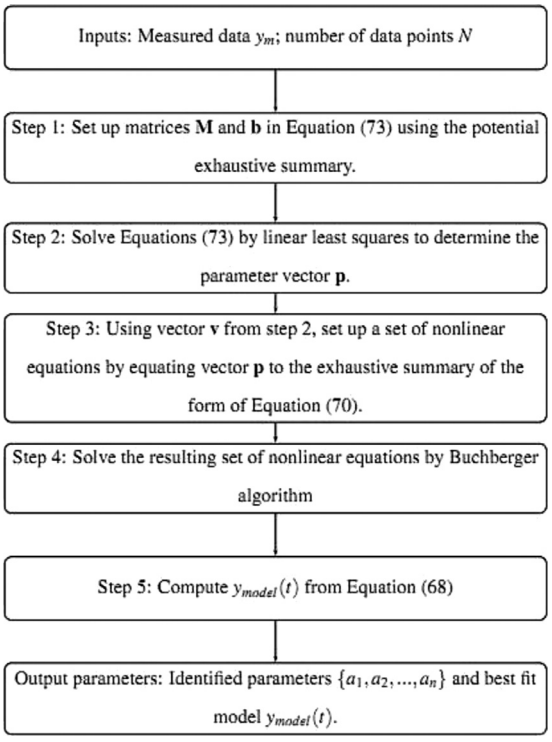

Fig. 5. Algorithm for identifying parameters $\{a_1, a_2, \ldots, a_n\}$ of Eq. (66) from measured data using the potential jet space identifiability theory.

infusion rate (mU/min); p_G the time varying fractional clearance of plasma glucose at basal insulin (min^{-1}); S_I the time varying insulin sensitivity (L/mU min); and α_G the Michealis–Menten parameter for glucose clearance saturation.

The parameter $Q(t)$ in Eq. (79) can be estimated by treating k as a fixed known population parameter representing the average patient response. Sensitivity analysis has shown that within physical ranges this assumption does not significantly affect the results of identifying p_G and S_I in clinical applications [13,14,21]. Applying the integral operator of Eq. (47) with $k = 1$ onto Eq. (78) yields:

$$G(t) - G(0) = -p_G \int_0^t G\, dt - S_I \int_0^t (G + G_E)\overline{Q}\, dt + \int_0^t P(t)\, dt \tag{80}$$

Eq. (80) is the potential jet space input–output equation with potentials:

$$\frac{dz_1}{dt} = G, \quad \frac{dz_2}{dt} = (G + G_E)\overline{Q}, \tag{81}$$

and can be used to identify p_G and S_I, which corresponds to the integral method as detailed in Ref. [22].

3. Results and discussion

3.1. Application to linear anesthetic uptake model

3.1.1. Modeling of nitrous oxide (N_2O) uptake and data acquisition

Consider a linear model of nitrous oxide (N_2O) uptake from Ref. [38], with the following kinetics of uptake and distribution, defined by the following differential rate equations:

$$\begin{aligned}
\dot{x}_1 &= k_{01} + k_{21}x_2 + k_{31}x_3 - (k_{10} + k_{12} + k_{13})x_1 \\
\dot{x}_2 &= k_{12}x_1 - k_{21}x_2 \\
\dot{x}_3 &= k_{13}x_1 - k_{31}x_3
\end{aligned} \tag{82}$$

where $k_{01} \equiv u_{00} = 1.43929$ denotes the rate of constant input into the central compartment x_1, k_{10} the rate of loss from the central compartment, k_{12} and k_{21} the rate of transfer of anesthetics from central compartment into the second compartment x_2, k_{13} and k_{31} the rate of transfer of anesthetics from central compartment into the third compartment x_3.

The rate equations of Eq. (82) are combined into a single third order linear differential equation of the form:

$$\dddot{x}_1 + b\ddot{x}_1 + c\dot{x}_1 + dx_1 = f \tag{83}$$

where the rate constants are related to the rate constants of Eq. (82) by:

$$b = k_{10} + k_{12} + k_{13} + k_{21} + k_{31} \tag{84}$$
$$c = k_{31}(k_{10} + k_{12} + k_{21}) + k_{21}(k_{10} + k_{13}) \tag{85}$$
$$d = k_{31}(k_{13}(k_{31} - k_{21}) + k_{21}(k_{10} + k_{13}) - k_{31}k_{13}) \tag{86}$$
$$f = k_{21}k_{31}k_{01} \tag{87}$$

To determine the dynamics of anesthetic uptake, Eq. (83) is solved subjected to the following initial conditions:

$$x_1(0) = 0, \quad \dot{x}_1(0) = k_{01}, \quad \ddot{x}_1(0) = -(k_{12} + k_{10} + k_{13})k_{01} \tag{88}$$

The complete analytical solution is of the form:

$$y(t) = \frac{f}{d} + A_1 \exp(r_1 t) + A_2 \exp(r_2 t) + A_3 \exp(r_3 t) \tag{89}$$

where A_1, A_2 and A_3 are determined by the initial conditions, and r_1, r_2, r_3 are the roots of the characteristic equation:

$$r^3 + br^2 + cr + d = 0 \tag{90}$$

The reported values for the seven constants $\{\frac{f}{d}, A_1, A_2, A_3, r_1, r_2, r_3\}$ for the case of nitrous oxide (N_2O) uptake from Ref. [38] are:

$$\begin{aligned}
&\frac{f}{d} = 0.910, \quad A_1 = -0.522, \quad A_2 = -0.343, \quad A_3 = -0.055, \\
&r_1 = -2.50, \quad r_2 = -0.388, \quad r_3 = -0.022
\end{aligned} \tag{91}$$

The corresponding rate constants $\{k_{10}, k_{12}, k_{13}, k_{21}, k_{31}\}$ are determined from the equations:

$$\begin{aligned}
A_1 + A_2 + A_3 &= -\frac{f}{d} \\
A_1r_1 + A_2r_2 + A_3r_3 &= k_{01} \\
A_1r_1^2 + A_2r_2^2 + A_3r_3^2 &= -(k_{12} + k_{10} + k_{13})k_{01} \\
r_1^3 + br_1^2 + cr_1 + d &= 0 \\
r_2^3 + br_2^2 + cr_2 + d &= 0 \\
r_3^3 + br_3^2 + cr_3 + d &= 0
\end{aligned} \tag{92}$$

Note that Eq. (92) is of the form:

$$\mathbf{f}(k_{01}, k_{10}, k_{12}, k_{21}, k_{13}, k_{31}) = \mathbf{0} \tag{93}$$

Eq. (92) is solved using the Buchberger algorithm to generate the following equivalent constants for the model defined in Eq. (82):

$$\begin{aligned}
&k_{01} = 1.43929, \quad k_{10} = 1.56445, \quad k_{12} = 0.644619, \\
&k_{13} = 0.09356 \quad k_{21} = 0.58401, \quad k_{31} = 0.023356
\end{aligned} \tag{94}$$

The constants of Eq. (94) are derived from physical measurement of N_2O uptake [38] with the addition of measurement noise, and are used to prove the concept of practical identifiability theory proposed in this paper.

A common method of measuring alveolar-to-inspired concentrations of N_2O is mass spectroscopy, which involves using a mass spectrometer to analyze the inhalational anesthetic agents on breath to breath [1]. This method is known to have an approximately Gaussian shaped distribution [42]. Therefore, for the analysis in this paper, a simple Gaussian noise model on the output data y is assumed. The model is:

$$\text{Noise model:} \quad y_{\text{noise}}(t) = y_m(t)\left(1 + \frac{\eta}{100}\epsilon\right), \quad \eta = 3. \tag{95}$$

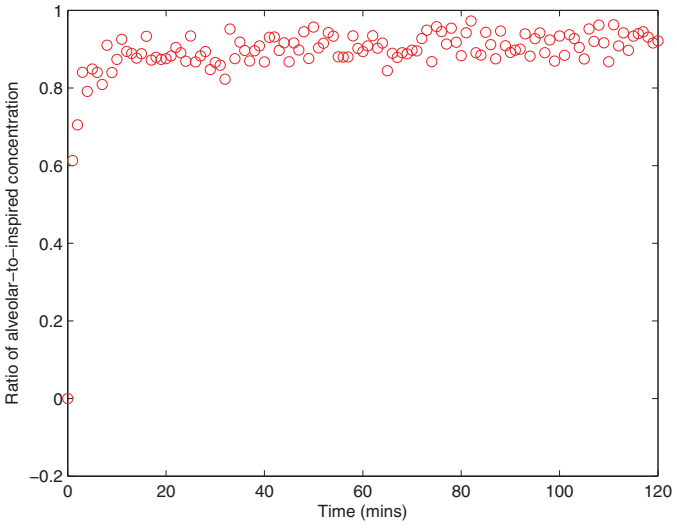

Fig. 6. Adding noise to the simulated data using noise model of Eqs. (95)–(96).

$$\epsilon \equiv \text{Random number from the Gaussian distribution,}$$
$$\mu = 0, \quad \sigma = 1.0 \tag{96}$$

This is a common model of noise for concentrations in the plasma where the higher the concentration is, the greater is the noise. The value of the noise level η is fixed at 3 to keep the coefficient of variation to 0.03 which is stated in Ref. [1]. An example of adding noise to the uptake data is shown in Fig. 6.

3.1.2. Differential jet space analysis

The system matrix $\mathbf{A_3}$ is:

$$\mathbf{A_3} = \begin{bmatrix} -(k_{10}+k_{12}+k_{13}) & k_{21} & k_{31} \\ k_{12} & -k_{21} & 0 \\ k_{13} & 0 & -k_{31} \end{bmatrix} \tag{97}$$

The differential input–output equation is obtained by constructing the augmented matrix equation of Eq. (34) with $n = 3$, as was done for the example case with $n = 2$. The substitution equation for this system is:

$$\dot{x}_1 = -(k_{10}+k_{12}+k_{13})x_1 + k_{21}x_2 + k_{31}x_3 + k_{01}u(t) \tag{98}$$

The final augmented matrix system of the form described in Eq. (34) is:

$$\mathbf{M} = \begin{bmatrix} 0 & 0 & k_{21} & k_{31} & 0 & 0 & 0 & 0 \\ 0 & 0 & 0 & 0 & 0 & 0 & 0 & 0 \\ -k_{21} & 0 & -1 & 0 & 0 & 0 & 0 & 0 \\ 0 & -k_{31} & 0 & -1 & 0 & 0 & 0 & 0 \\ 0 & 0 & -k_{21} & 0 & -1 & 0 & 0 & 0 \\ 0 & 0 & 0 & -k_{31} & 0 & -1 & 0 & 0 \\ 0 & 0 & 0 & 0 & -k_{21} & 0 & -1 & 0 \\ 0 & 0 & 0 & 0 & 0 & -k_{31} & 0 & -1 \end{bmatrix} \tag{99}$$

$$\overline{\mathbf{X}} = \begin{bmatrix} x_2 \\ x_3 \\ \dot{x}_2 \\ \dot{x}_3 \\ \ddot{x}_2 \\ \ddot{x}_3 \\ \dddot{x}_2 \\ \dddot{x}_3 \end{bmatrix}, \quad \mathbf{B} = \begin{bmatrix} \ddot{x}_1 + (k_{10}+k_{12}+k_{13})\dot{x}_1 - k_{01}\dot{u} \\ \dddot{x}_1 + (k_{10}+k_{12}+k_{13})\ddot{x}_1 - k_{01}\ddot{u} \\ k_{12}x_1 \\ k_{13}x_1 \\ k_{12}\dot{x}_1 \\ k_{13}\dot{x}_1 \\ k_{12}\ddot{x}_1 \\ k_{13}\ddot{x}_1 \end{bmatrix} \tag{100}$$

Solving the augmented matrix equation using the matrices defined in Eq. (99) and (100), yields the unknown states $\overline{\mathbf{X}}$ of Eq. (100). These unknown states are substituted back into Eq. (98), as was done with the 2-compartment case, to yield the following input–output equation:

$$\begin{aligned}&(k_{10}-k_{21}-k_{12}-k_{13}-k_{31})\,\ddot{y} \\ &\quad + (-k_{10}k_{21}-k_{12}k_{31}-k_{21}k_{31}-k_{13}k_{21}-k_{10}k_{31})\,\dot{y} \\ &\quad + u_{00}k_{21}k_{31} - k_{10}k_{21}k_{31}\,y - \dddot{y} = 0\end{aligned} \tag{101}$$

Note that Eq. (101) is in the form of Eq. (83) with the constants given in Eq. (94). Thus, for simplicity the differential input–output equation is defined by Eq. (83) with $y(t) \equiv x_1$.

To identify the unknown parameters $\{b, c, d, f\}$ from the simulated uptake data using the differential jet space analysis, Eq. (83) is rearranged into an equation of the form:

$$\dddot{y} = -b\ddot{y} - c\dot{y} - dy + f \tag{102}$$

where all the derivatives are numerically evaluated by finite differences. Set $y = y_{\text{data}}(t)$ into Eq. (102), and substitute various values of t for $t \in \{t_1, \ldots, t_N\}$ into Eq. (102), yields a set of N equations in 4 unknowns, which is described by the following matrix equation:

$$\mathbf{M_{d\text{-}jet}}\,\mathbf{p} = \mathbf{b_{d\text{-}jet}} \tag{103}$$

where:

$$\mathbf{M_{d\text{-}jet}} = \begin{bmatrix} -\ddot{y}(1) & -\dot{y}(1) & -y(1) & 1 \\ -\ddot{y}(2) & -\dot{y}(2) & -y(2) & 1 \\ \vdots & \vdots & \vdots & \vdots \\ -\ddot{y}(N) & -\dot{y}(N) & -y(N) & 1 \end{bmatrix} \equiv \text{coefficients from differential jet space formulation} \tag{104}$$

$$\mathbf{p} = \begin{bmatrix} b \\ c \\ d \\ f \end{bmatrix}, \quad \mathbf{b_{d\text{-}jet}} = \begin{bmatrix} \dddot{y}(1) \\ \dddot{y}(2) \\ \vdots \\ \dddot{y}(N) \end{bmatrix} \tag{105}$$

Solving Eqs. (103) and (104) by linear least squares determines the best fit to the differential input–output equation.

3.1.3. Potential jet space analysis

To obtain the potentials input–output equation, the one-to-one relationship between the differential jet space method and the potential jet space method is exploited. In this light, Eq. (83) is operated on by the operator $I^{(3)}(X)$, which yields:

$$\begin{aligned}&y - y_0 - (dy_0 + b\,y_0)\,t - (ddy_0 - b\,dy_0 - c\,y_0)\frac{t^2}{2!} - b\int_0^t y\,\mathrm{d}t \\ &\quad - c\int_0^t\int_0^t y\,\mathrm{d}t\,\mathrm{d}t - d\int_0^t\int_0^t\int_0^t y\,\mathrm{d}t\,\mathrm{d}t\,\mathrm{d}t + \frac{ft^3}{3!} = 0\end{aligned} \tag{106}$$

where y_{0b} denotes the initial condition of the data, dy_0 the derivative initial condition, and ddy_{0b} the second order derivative initial condition. These initial conditions are treated as extra unknowns.

Eq. (106) can be rearranged to obtain a formulation of $y_{\text{model}}(t)$:

$$\begin{aligned}y_{\text{model}}(t) = y_0 + d\bar{y}_0\,t + d^2\bar{y}_0\,\frac{t^2}{2!} + b\int_0^t y\,\mathrm{d}t + c\int_0^t\int_0^t y\,\mathrm{d}t\,\mathrm{d}t \\ + d\int_0^t\int_0^t\int_0^t y\,\mathrm{d}t\,\mathrm{d}t\,\mathrm{d}t - f\,\frac{t^3}{3!}\end{aligned} \tag{107}$$

where:

$$d\bar{y}_0 = dy_0 + by_0 \tag{108}$$

$$d^2\bar{y}_0 = \frac{d^2y_0 - b\,d\bar{y}_0 + b^2y_0 + cy_0}{2} \tag{109}$$

To construct the exhaustive summary for the input–output equations of Eq. (106), the coefficients of the input–output equations are extracted and evaluated at the symbolic parameter values $\mathbf{p_3} = [m_1, m_2, m_3, -m_4, -m_5, -m_6, -m_7]^T$ which yields the following set of algebraic nonlinear equations:

$$\{y_0 - m_1,\ \ dy_0 + by_0 - m_2,\ \ ddy_0 - b\,dy_0 - c\,y_0 - m_3,\\ b - m_4,\ \ c - m_5,\ \ d - m_6,\ \ f - m_7\} \tag{110}$$

The set of exhaustive summary of Eq. (110) has a unique solution so the parameters b, c, d and f in Eq. (83) are identifiable. However, although b, c, d and f can be identified, these parameters depend on 6 parameters in Eqs. (84)–(87). Thus, in terms of the rate constants $\{k_{10}, k_{01}, k_{12}, k_{21}, k_{13}, k_{31}\}$ the anesthetic uptake model is unidentifiable unless 2 of these values are held constant. Therefore, assuming $k_{01} = 1.43929$, $k_{10} = 1.56445$ it is theoretically possible to identify the parameters k_{12}, k_{21}, k_{13} and k_{31}.

Set $y_{\text{model}}(t) = y_{\text{data}}(t)$ in Eq. (107), and choose $t \in \{t_1, \ldots, t_N\}$ to yield a set of N equations in 7 unknowns, as was done in the setup of Eq. (72). The resulting matrix equation is:

$$\mathbf{M_{p\text{-}jet}}\ \mathbf{p} = \mathbf{b_{p\text{-}jet}} \tag{111}$$

$$\mathbf{M_{p\text{-}jet}} = \left[\mathbf{M_{3,1}}|\mathbf{M_{3,2}}|\mathbf{M_{3,3}}|\mathbf{M_{3,4}}|\mathbf{M_{3,5}}|\mathbf{M_{3,6}}|\mathbf{M_{3,7}}\right] \tag{112}$$

$$\mathbf{M_{3,1}} = \mathbf{1_{N\times 1}} \quad \mathbf{M_{3,2}} = \mathbf{T_{N\times 1}}, \quad \mathbf{M_{3,3}} = \mathbf{T^2_{N\times 1}} \tag{113}$$

$$\mathbf{M_{3,4}} = I^{(1)}\,\mathbf{y_{N\times 1}}, \quad \mathbf{M_{3,5}} = I^{(2)}\,\mathbf{y_{N\times 1}},\\ \mathbf{M_{3,6}} = I^{(3)}\,\mathbf{y_{N\times 1}}, \quad \mathbf{M_{3,7}} = \mathbf{T^3_{N\times 1}} \tag{114}$$

$$\mathbf{1_{N\times 1}}, \mathbf{T_{N\times 1}} \equiv \text{Eq.(74)}, \quad \mathbf{W_{N\times 1}}, I^{(i)}\,\mathbf{W_{N\times 1}} \equiv \text{Eq.(77)} \tag{115}$$

$$\mathbf{p} = \begin{bmatrix} y_0 \\ dy_{0b} \\ ddy_{0b} \\ b \\ c \\ d \\ f \end{bmatrix}, \quad \mathbf{b_{p-jet}} = \begin{bmatrix} y_{\text{meas}}(t_1) \\ \vdots \\ y_{\text{meas}}(t_N) \end{bmatrix} \tag{116}$$

Solving Eqs. (111)–(116) by linear least squares, determines the values for the vector $\mathbf{v_{pot3}}$, which corresponds to the best model fit to the N_2O uptake data.

3.1.4. Parameter identification of N_2O uptake-differential versus potential jet space

To test the performance of both the differential and potential jet space methods under the presence of noise, the noise model of Eqs. (95) and (96) is used. Define the following metric to measure the error in the fit of the model:

$$e_\eta = \underset{t}{\text{mean}}\,|y_{\text{meas}}(t) - y_{\text{model}}(t)|,\\ \eta = 3 \text{ is noise level in percentage from Ref. [1]} \tag{117}$$

Note that Eq. (117) is used primarily since it has a more direct physical interpretation however it has been shown to be less sensitive to outliers than the popular root-mean-square-error metric [4]. Define the mean absolute percentage error metric:

$$e_{\eta,p} = \frac{\underset{t}{\text{mean}}\,|y_{\text{meas}}(t) - y_{\text{model}}(t)|}{|y_{\text{meas}}(t)|} \times 100,\\ \eta = 3 \text{ is percentage noise level from Ref. [1]} \tag{118}$$

Table 1
Comparing the identified parameters of the N_2O model against the true parameters for noise level of 3%.

Parameter	True value	Differential jet space	Potential jet space
b	2.8900	$[-0.1086\times10^{-6}, 0.1666\times10^{-6}]$	[2.6934,2.943]
c	1.0126	$[-0.1083\times10^{-6}, -0.0211\times10^{-6}]$	[1.0015,1.0267]
d	0.0181	$[-0.6800\times10^{-7}, 0.4551\times10^{-7}]$	[0.0171,0.0193]
f	0.0167	$[-0.6002\times10^{-7}, 0.3791\times10^{-7}]$	[0.0160,0.0174]

Table 2
Comparing model response errors η given in Eq. (117) of the identified curves in comparison to the true curve, for noise level of 3% for differential and potential jet space approaches. The numbers in parentheses represent mean absolute percentage error defined in Eq. (118)

	Differential jet space	Potential jet space
Model response error η	[7851, 7870]	[0.0199 (2.2%), 0.0249 (2.9%)]

For the given noise level, 100 Monte Carlo simulations were conducted and the mean value of e_η is calculated for both the differential jet space and the potential jet space models. Table 1 shows the comparison between 90% confidence interval of the identified lumped parameters b, c, d and f, for differential and potential jet space approaches respectively, against the true parameters. Table 2 shows the 90% confidence interval of the error, for the differential and potential jet space approaches. It is clear from Table 1 that the identified parameters b, c, d and f for the differential jet space approach are significantly different from the true values, while the identified parameters for the potential jet space approach tightly surround the true values. Table 2 shows that the potential jet space model match is close to 1% of the zero noise case, and lies well within the coefficient of variation for all t; whereas the differential jet space model match becomes unbounded with the presence of noise. Fig. 7 shows the match of the potential jet space approach for the case of 10% noise. It is seen that even at a significantly high level of noise, the potential jet space model match is close to the true model. The major reason for this robustness in the presence of significant noise, is that the formulation is in terms of integrals of the measured data. These integrals provide a filter based on the dynamics of the underlying equation, and therefore no specific noise or disturbance model is required.

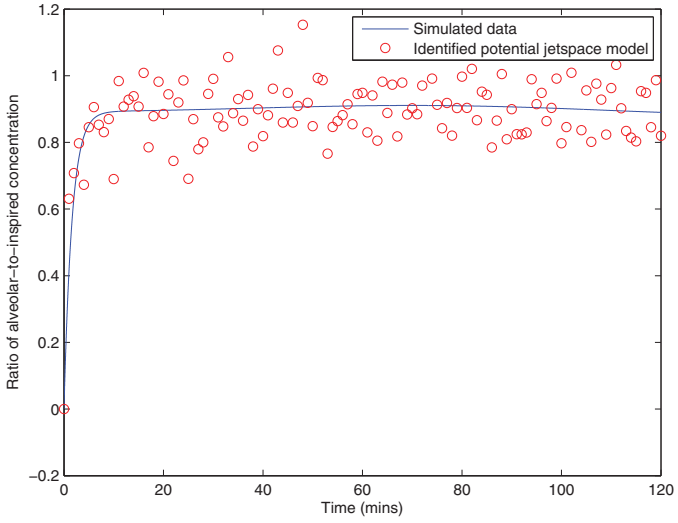

Fig. 7. Comparison between the simulated response and identified model from the potential jet space approach of alveolar-to-inspired concentration ratio of nitrous oxide (N_2O) at 10% level of noise.

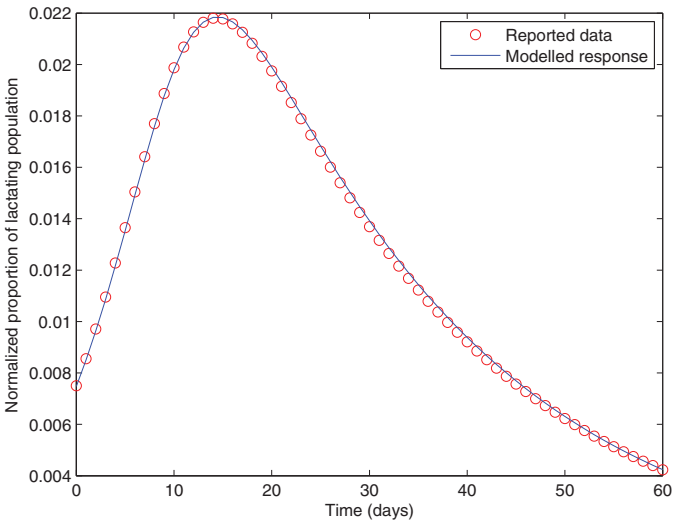

Fig. 8. Comparison between the model response of normalized proportion of lactating population in cows versus reported data.

3.2. Potential jet space approach for nonlinear systems

3.2.1. Modeling and data acquisition

Consider the following example from an immunological model for mastitis in dairy cows. This model was introduced in Doepfer [16], and reproduced in Margaria *et al.* [31]:

$$\begin{aligned}\dot{x}_1 &= p_1 x_1 - p_2 x_1 x_2\\ \dot{x}_2 &= p_3 x_2 (1 - p_4 x_2) + p_5 x_1 x_2\end{aligned} \tag{119}$$

To prove the concept the following parameters are chosen to provide a response that is approximately similar to the magnitudes given in [8]:

$$p_1 = 0.5 \quad p_2 = 1.2 \quad p_3 = 2.78, \quad p_4 = 0.7 \quad p_5 = 0.3 \tag{120}$$

The initial conditions are:

$$x_1(0) \equiv y_0 = 0.0075, \quad \dot{x}_1(0) \equiv dy_0 = 0.005 \tag{121}$$

Data of the infected population is taken once a day for a period of 60 days and the model response is given in Fig. 8. The y axis is the normalized proportion of lactating population infected with pathogens.

3.2.2. Potential jet space analysis and identification

Applying the differential jet space analysis to the system in Eq. (119) in similar fashion as was done in Jirstrand [26] gives the following input–output equation:

$$\begin{aligned}&p_2\, y\, \ddot{y} - (p_2 + p_3 p_4)\, \dot{y}^2 + (2 p_1 p_3 p_4 - p_2 p_3)\, y \dot{y} - p_2 p_5\, y^2 \dot{y}\\ &\quad + (p_1 p_2 p_3 - p_1^2 p_3 p_4)\, y^2 + p_1 p_2 p_5\, y^3 = 0\end{aligned} \tag{122}$$

Eq. (122) is made monic by dividing through by parameter p_2 to yield:

$$\begin{aligned}&y\, \ddot{y} - \frac{(p_2 + p_3 p_4)}{p_2}\, \dot{y}^2 + \frac{(2 p_1 p_3 p_4 - p_2 p_3)}{p_2}\, y \dot{y} - p_5\, y^2\, \dot{y}\\ &\quad + \frac{(p_1 p_2 p_3 - p_1^2 p_3 p_4)}{p_2}\, y^2 + p_1 p_5\, y^3 = 0\end{aligned} \tag{123}$$

The signal y is the normalized proportion of lactating population infected with pathogens, and hence is always positive, assuming a non-zero starting point. Therefore, Eq. (123) is written in the form:

$$\ddot{y} + a \frac{\dot{y}^2}{y} + b\, \dot{y} + c\, y\, \dot{y} + d\, y + e\, y^2 = 0 \tag{124}$$

where:

$$\begin{aligned}a &= -\frac{(p_2 + p_3 p_4)}{p_2}, \quad b = \frac{(2 p_1 p_3 p_4 - p_2 p_3)}{p_2}, \quad c = -p_5\\ d &= \frac{(p_1 p_2 p_3 - p_1^2 p_3 p_4)}{p_2}, \quad e = p_1 p_5\end{aligned} \tag{125}$$

Integrating Eq. (124) twice with respect to time, yields:

$$\begin{aligned}&y - y_0 - dy_0 t + a \int_0^t \int_0^t \frac{\dot{y}^2}{y}\, dt\, dt + b \int_0^t (y - y_0)\, dt\\ &+ \frac{c}{2} \int_0^t (y^2 - y_0^2)\, dt + d \int_0^t \int_0^t y\, dt\, dt + e \int_0^t \int_0^t y^2\, dt\, dt = 0\end{aligned} \tag{126}$$

$$\begin{aligned}y_{\text{model}}(t) &= y_0 + dy_0 t - a \int_0^t \int_0^t \frac{\dot{y}^2}{y}\, dt\, dt - b \int_0^t (y - y_0)\, dt\\ &- \frac{c}{2} \int_0^t (y^2 - y_0^2)\, dt - d \int_0^t \int_0^t y\, dt\, dt - e \int_0^t \int_0^t y^2\, dt\, dt\end{aligned} \tag{127}$$

where y_0 and dy_0 denote the initial conditions. Note that the double integrals of the expressions involving the first derivative in Eqs. (126) and (127) are effectively equivalent to a single integral of an expression involving measured data and no derivatives. Thus, the effect of the derivative in the overall formulation is to add a potential jet space term of order 1. Since this term is still effectively an integral, the extra noise involved with differentiating the data is removed. Monte Carlo simulations with noise further demonstrate this concept below. Eq. (127) can be further rewritten in terms of potentials:

$$\begin{aligned}y_{\text{model}}(t) &= y_0 + dy_0 t - a\,(t\, z_1 - z_1) - b\,(z_2 - y_0\, t)\\ &- \frac{c}{2}\,(z_3 - y_0^2\, t) - d\,(t\, z_2 - z_2) - e\,(t\, z_3 - z_3)\end{aligned} \tag{128}$$

where:

$$\frac{dz_1}{dt} = \frac{\dot{y}^2}{y}, \quad \frac{dz_2}{dt} = y, \quad \frac{dz_3}{dt} = y^2 \tag{129}$$

Identification of the lumped parameters described in Eq. (125) from a set of simulated data is achieved by setting $y_{\text{model}}(t) = y_{\text{data}}(t)$ in Eq. (127). Values of t for $t \in \{t_1, \ldots, t_N\}$ are substituted into Eq. (127), assuming that $y_0 = y_{\text{meas}}(t_1)$, to yield a set of N equations in 6 unknowns. The matrix equation is:

$$\mathbf{M_{nonlin}}\ \mathbf{p} = \mathbf{b_{nonlin}}, \tag{130}$$

where:

$$\mathbf{M_{nonlin}} = \left[\mathbf{T}_{N\times 1}\ I^{(2)}\frac{\dot{\mathbf{y}}^2}{\mathbf{y}}\ I^{(1)}(\mathbf{y} - y_0)\ \tfrac{1}{2} I^{(1)}(\mathbf{y}^2 - y_0^2)\ I^{(2)}\mathbf{y}\ I^{(2)}\mathbf{y}^2\right] \tag{131}$$

$$\mathbf{p} = \begin{bmatrix} dy_0 \\ a \\ b \\ c \\ d \\ e \end{bmatrix}, \qquad \mathbf{b_{nonlin}} = \begin{bmatrix} y_{\text{meas}}(1) - y_0 \\ \vdots \\ y_{\text{meas}}(t_N) - y_0 \end{bmatrix} \tag{132}$$

$$\mathbf{T}_{N\times 1},\ I^{(i)}\mathbf{W}_{N\times 1} \equiv \text{Eq.(115)} \tag{133}$$

However, even though the parameter vector $\mathbf{p}$ in Eq. (132) is theoretically identifiable it has been found in numerical simulation that setting $p_5 = 0$ in Eq. (125) has negligible effect on the resulting match to the data. This result shows a limitation on the identifiability theory which does not include measurement noise in the analysis. Therefore the theory cannot find parameters that may have a very limited effect on the model response and thus give indistinguishable changes of the response within the noise envelope. This problem is common in

physiological modeling, and further justifies the development of an identifiability theory that works in practice. Setting $p_5 = 0$ is equivalent to setting $c = 0$ and $e = 0$. Therefore, in the identification of parameters, c and e are fixed at zero throughout even though the true values are non-zero. A further constraint is that $a < 0$, which is clear from Eq. (125).

The procedure for determining the lumped parameters a, b and d of the model in Eq. (127) solves Eqs. (130)–(132) by linear least squares for the full parameter vector subjected to the following matrix constraints:

$$\mathbf{A_{leq}p} < \mathbf{b_{leq}} \tag{134}$$

$$\mathbf{A_{eq}p} = \mathbf{b_{eq}} \tag{135}$$

where:

$$\mathbf{A_{leq}} = \begin{bmatrix} 0 & 1 & 0 & 0 & 0 & 0 \end{bmatrix}, \quad \mathbf{b_{leq}} = \begin{bmatrix} 0 & 0 & 0 & 0 & 0 & 0 \end{bmatrix} \tag{136}$$

$$\mathbf{A_{eq}} = \begin{bmatrix} 0 & 0 & 0 & 1 & 0 & 0 \\ 0 & 0 & 0 & 0 & 0 & 1 \end{bmatrix}, \quad \mathbf{b_{eq}} = \begin{bmatrix} 0 \\ 0 \end{bmatrix} \tag{137}$$

Solving Eqs. (130)–(132) for the no-noise case gives a solution for the elements of vector $\mathbf{p}$ as follows:

$$\mathbf{p_{sol}} = \begin{bmatrix} \hat{dy}_0 \\ -2.4338 \\ 0.1502 \\ 0 \\ 0.0082 \\ 0 \end{bmatrix}, \quad \hat{dy}_0 = 0.0009 \tag{138}$$

The parameters $\mathbf{p} = \mathbf{p_{sol}}$ in Eq. (138) are used to resimulate the original differential equation to produce $\{C_1$ = curve with parameters $\mathbf{p_{sol}}$, $dy_0 = \hat{dy}_0\}$. As a comparison the same parameters are used except that dy_0 is replaced by the true derivative initial condition $dy_0 = dy_{0,\text{true}}$, to produce $\{C_2$ = curve with parameters $\mathbf{p_{sol}}$, $dy_0 = dy_{0,\text{true}}\}$. Both curves are given in Fig. 9. The result of Fig. 9 shows that even though the derivative is identified with reasonable accuracy (10% error) this error is greatly magnified after simulation. This dynamic is not related to noise or the potential jet space method, it is an inherent part of the dynamic response and is only related to the model itself. However, the parameters a, b and d have been successfully identified independent of this initial derivative effect and the assumptions of $c = 0$ and $e = 0$ had very little effect on the result. Note that the use of a standard finite difference to estimate the derivative would give a much greater error in the first derivative as it only uses local information. The formulation of Eqs. (130)–(132) is a different concept to finite differences as it is an integral formulation of the differential equation model that utilizes the global data set and is thus much less sensitive to noise.

Notice that the peak of C_2 significantly overshoots the data in Fig. 9. This result suggests that data up to the peak would be sufficient to identify the derivative initial condition more accurately. Consider an initial approximated model $y_{\text{model},1}(t)$ which is obtained by substituting the identified parameters from vector $\mathbf{p_{sol}}$ into the integral model of Eq. (127):

$$y_{\text{model},1}(t) = y_0 + dy_0\, t - \hat{a} \int_0^t \int_0^t \frac{\dot{y}^2}{y}\, dt\, dt - \hat{b} \int_0^t (y - y_0) dt - \hat{d} \int_0^t \int_0^t y\, dt\, dt \tag{139}$$

where $\hat{a} = -2.4338$, $\hat{b} = 0.1502$, $\hat{d} = 0.0082$. Setting $y_{\text{model},1}(t) = y_{\text{meas}}(t)$ in Eq. (139) and substituting $t \in \{t_1, \ldots, t_N\}$ into Eq. (139) yield a set of N equations in 2 unknowns which is represented by the matrix equation:

$$\mathbf{M_{iter}} \begin{bmatrix} y_{0c} \\ dy_{0c} \end{bmatrix} = \mathbf{b_{iter}} \tag{140}$$

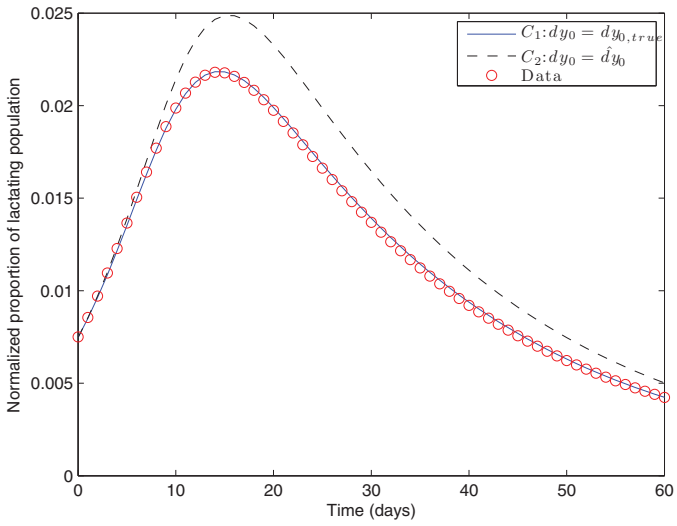

Fig. 9. Comparison between the simulated data to two sets of curves defined by two different sets of initial conditions, $dy_0 = 0.0009$ and $dy_0 = dy_{0,\text{true}}$ respectively.

where:

$$\mathbf{M_{iter}} = \left[\mathbf{1_{N_p \times 1}} + \hat{b}\, \mathbf{T_{N \times 1}} \middle|\, \mathbf{T_{N \times 1}} \right] \tag{141}$$

$$\mathbf{b_{iter}} = \begin{bmatrix} y_{\text{meas}}(1) - \left(-\hat{a} \int_0^{t_1} \int_0^{t_1} \frac{\dot{y}_{\text{model},1}^{\,2}}{y_{\text{model},1}}\, dt\, dt - \hat{b} \int_0^{t_1} y_{\text{model},1}(t)\, dt - \hat{d} \int_0^{t_1} \int_0^{t_1} y_{\text{model},1}(t)\, dt\, dt \right) \\ \vdots \\ y_{\text{meas}}(N) - \left(-\hat{a} \int_0^{t_N} \int_0^{t_N} \frac{\dot{y}_{\text{model},1}^{\,2}}{y_{\text{model},1}}\, dt\, dt - \hat{b} \int_0^{t_N} y_{\text{model},1}(t)\, dt - \hat{d} \int_0^{t_N} \int_0^{t_N} y_{\text{model},1}(t)\, dt\, dt \right) \end{bmatrix} \tag{142}$$

where $\mathbf{1_{N \times 1}}$ and $\mathbf{T_{N \times 1}}$ are defined in Eq. (74). Solving Eqs. (140)–(142) by linear least squares gives an updated estimate of the initial conditions y_{0c}, and dy_{0c}. These estimates are substituted into the integral model of Eq. (139), to arrive at the next approximate integral model. This algorithm is iterated until convergence is reached. Note that the updating part of this iterative approach is similar to a Picard iteration, but the overall approach is different since the original Picard iteration only solves the differential equation for fixed initial condition and parameters. The resulting initial conditions are used to resimulate the curve and the result is a reduction in mean error from 16% to 1%. This result further shows the versatility and robustness of working in the potential jet space, as this process would not work in the differential jet space. This sensitivity in the initial derivative would also greatly affect standard non-linear regression methods, as the resolution in the step size for the unknown derivative would have to be significantly reduced which would greatly increase the computation required. In contrast, the iteration on the potential jet space is very computationally efficient as it does not require the solving of the differential equation for every new update in the estimated parameters.

To further prove the concept, uncertainty and noise in these measurements are described by the simple Gaussian noise model of Eqs. (95) and (96) with $\eta = 2, 5, 10$. Note that practical measurement

Table 3
Comparing the identified parameters of the non-linear mastitis model against the true parameters for 2%, 5% and 10% levels of noise.

Parameter	True value	Identified value (2%)	Identified value (5%)	Identified value (10%)
y_0	0.0075	[0.0072,0.0077]	[0.0068,0.0080]	[0.0059,0.0085]
dy_0	0.001	[0.0009,0.0011]	[0.0009,0.0013]	[0.0007,0.0014]
a	−2.3335	[−2.6777,−2.1588]	[−2.7832,−1.6401]	[−3.0558,−1.0522]
b	0.1500	[0.1419,0.1601]	[0.1266,0.1611]	[0.1043,0.1691]
d	0.0075	[0.0073,0.0090]	[0.0069,0.0092]	[0.0056,0.0113]

Table 4
Percentiles of the mean absolute response errors η given in Eq. (117) of the identified curves in comparison to the true curve, for noise levels up to 10%. The numbers in parentheses represent the mean absolute percentage errors of the form defined in Eq. (118).

Noise level (%)	Mean absolute errors (η)
2	[1.841×10^{-4}(1.53%), 2.3840×10^{-4}(1.98%)]
5	[4.146×10^{-4}(3.4%), 5.7510×10^{-4}(4.71%)]
10	[7.4×10^{-4}(6.1%), 1.13×10^{-3}(9.0%)]

of lactating proportions is carried out by placing a combination of indicators such as electrical conductivity (EC) and lactate dehydrogenase (LDH) near the herds to measure milk characteristics [3].

For noise levels of 2%, 5% and 10%, 100 Monte Carlo simulations are performed for the nonlinear mastitis model of Eq. (127). Table 3 depicts the comparison between 90% confidence interval of the identified lumped parameters of the non-linear mastitis model against the true parameters. The results show that the identified values are close to the true values.

Fig. 10 shows an example of the identified model match to the data with 10% noise. Table 4 shows the 90% confidence interval of the mean absolute errors of the identified curves in comparison to the true curve, for noise levels of 2%, 5% and 10% respectively. For noise levels of up to 10%, the mean absolute errors are within 8.3% which is within the noise envelope. These results illustrate the robustness of the integral method to noise.

3.2.3. Heteroscedastic noise

Heteroscedasticity involves changes in variance in the dependent variable across data. In practice, sensor noise heteroscedasticity in compartmental systems can occur by changing the measurement site of the sensor within the same compartment [17], or measuring in a different compartment [18]. However, note that the noise model of Eq. (95) is also heteroscedastic since higher concentrations would have greater noise. This noise response is quite common for sensors that measure concentrations in plasma.

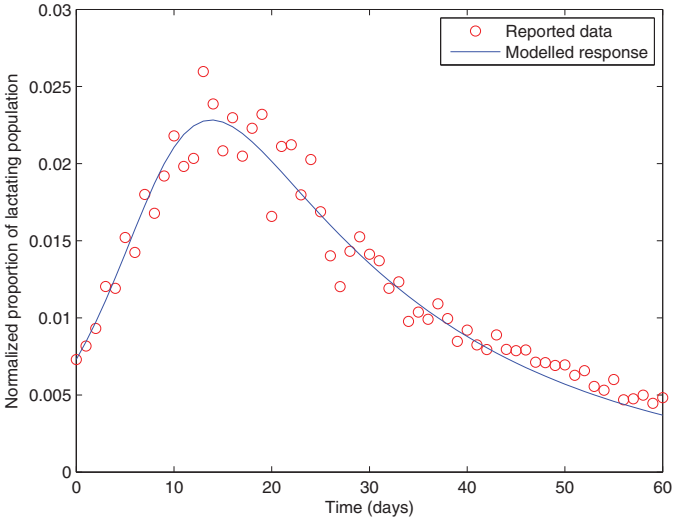

Fig. 10. Comparison between the model match of normalized proportion of lactating population in cows versus the simulated data at 10% noise.

Three experiments of the model in Eqs. (119) and (120) are performed defining by:

Experiment 1: Solution to Eqs. (119) and (120) with initial conditions $y_0 = 0.0075$, $dy_0 = 0.001$, and $\eta = 2$ in Eq. (95) (143)

Experiment 2: Solution to Eqs. (119) and (120) with initial conditions $y_0 = 0.1125$, $dy_0 = 0.0015$, and $\eta = 5$ in Eq. (95) (144)

Experiment 3: Solution to Eqs. (119) and (120) with initial conditions $y_0 = 0.1125$, $dy_0 = 0.002$, and $\eta = 10$ in Eq. (95) (145)

A different set of initial conditions is given in each experiment to represent different input rates of the disease into the cow population. The three levels of noise represent the heteroscedasticity across the experiments.

The procedure of identifying the mastitis model using potential jet space method begins with solving (130)–(132) by linear least squares method. For the heteroscedastic example investigated in this section, define a new $\mathbf{M_{nonlin}}$ matrix, and $\mathbf{b_{nonlin}}$ and $\mathbf{p}$ vectors of Eq. (131):

$$\mathbf{M_{nonlin}} = \begin{bmatrix} \kappa_1\mathbf{M_{nonlin,1}} \\ \kappa_2\mathbf{M_{nonlin,2}} \\ \kappa_3\mathbf{M_{nonlin,3}} \end{bmatrix}, \quad \mathbf{b_{nonlin}} = \begin{bmatrix} \kappa_1\mathbf{b_{nonlin,1}} \\ \kappa_2\mathbf{b_{nonlin,2}} \\ \kappa_3\mathbf{b_{nonlin,3}} \end{bmatrix} \tag{146}$$

where matrices $\mathbf{M_{nonlin,1}}$, $\mathbf{M_{nonlin,2}}$ and $\mathbf{M_{nonlin,3}}$ are defined:

$$\mathbf{M_{nonlin,1}} = \left[\mathbf{T}_{N\times1}\mathbf{0}_{N\times1}\mathbf{0}_{N\times1}I^{(2)}\frac{\dot{\mathbf{y}}^2_{\exp_1}}{\mathbf{y}_{\exp_1}}I^{(1)}(\mathbf{y}_{\exp_1} - y_{0,\exp_1}) \times \frac{1}{2}I^{(1)}(\mathbf{y}^2_{\exp_1} - y^2_{0,\exp_1})I^{(2)}\mathbf{y}_{\exp_1}I^{(2)}\mathbf{y}^2_{\exp_1} \right] \tag{147}$$

$$\mathbf{M_{nonlin,2}} = \left[\mathbf{0}_{N\times1}\mathbf{T}_{N\times1}\mathbf{0}_{N\times1}I^{(2)}\frac{\dot{\mathbf{y}}^2_{\exp_2}}{\mathbf{y}_{\exp_2}}I^{(1)}(\mathbf{y}_{\exp_2} - y_{0,\exp_2}) \times \frac{1}{2}I^{(1)}(\mathbf{y}^2_{\exp_2} - y^2_{0,\exp_2})I^{(2)}\mathbf{y}_{\exp_2}I^{(2)}\mathbf{y}^2_{\exp_2} \right] \tag{148}$$

$$\mathbf{M_{nonlin,3}} = \left[\mathbf{0}_{N\times1}\mathbf{0}_{N\times1}\mathbf{T}_{N\times1}I^{(2)}\frac{\dot{\mathbf{y}}^2_{\exp_3}}{\mathbf{y}_{\exp_3}}I^{(1)}(\mathbf{y}_{\exp_3} - y_{0,\exp_3}) \times \frac{1}{2}I^{(1)}(\mathbf{y}^2_{\exp_3} - y^2_{0,\exp_3})I^{(2)}\mathbf{y}_{\exp_3}I^{(2)}\mathbf{y}^2_{\exp3} \right] \tag{149}$$

$$\mathbf{b_{nonlin,i}} = \begin{bmatrix} y_{\text{meas},\exp_i}(1) - y_{0,\exp_i} \\ \vdots \\ y_{\text{meas},\exp_i}(t_N) - y_{0,\exp_i} \end{bmatrix}, \quad i = 1,2,3 \tag{150}$$

$$\mathbf{p} = \begin{bmatrix} dy_{0,\exp_1} \\ dy_{0,\exp_2} \\ dy_{0,\exp_3} \\ a \\ b \\ c \\ d \\ e \end{bmatrix} \tag{151}$$

Table 5
Comparing the identified parameters of the non-linear mastitis model, for the heteroscedastic noise example, against the true parameters.

Parameter	True value	Identified value (weighting (25,4,1))	Identified value (weighting (1,1,1))
$dy_{0,\exp_a}$	0.001	[0.0010, 0.0011]	[0.0011,0.0029]
$dy_{0,\exp_b}$	0.0015	[0.0014,0.0017]	[0.0017,0.0041]
$dy_{0,\exp_c}$	0.002	[0.0019,0.0023]	[0.0023,0.0058]
a	−2.3335	[−2.4938,−1.7289]	[−1.8298,0]
b	0.1500	[0.1315,0.1542]	[0.1066,0.1383]
d	0.0075	[0.0068,0.0084]	[0.0041,0.0074]

Table 6
Comparing the identified parameters of the non-linear mastitis model, for the heteroscedastic noise example, against the true parameters.

Experiment	Mean absolute errors		Maximum value
	Weighting (25,4,1)	Weighting (1,1,1)	
1	$[1.559\times10^{-4},2.227\times10^{-4}]$	$[2.559\times10^{-4},3.424\times10^{-4}]$	0.0211
2	$[4.049\times10^{-4},5.398\times10^{-4}]$	$[7.049\times10^{-4},8.966\times10^{-4}]$	0.0332
3	$[8.599\times10^{-4},9.654\times10^{-4}]$	$[1.5\times10^{-3},1.6\times10^{-3}]$	0.046

The scalars $\kappa_i \geq 0, i = 1, 2, 3$ are multiplicative weights, which are chosen arbitrarily with respect to the size of the variance for each experiment. For the three experiments described in this work, the multiplicative weights are $\kappa_1 = 25 \equiv (2^2 \times 2.5^2)$, $\kappa_2 = 4 \equiv 2^2$ and $\kappa_3 = 1$. These values are chosen to be in line with the squares of the errors.

The constraints in Eqs. (136) and (137) are also redefined to accommodate the augmentation of the three experiments:

$$\mathbf{A_{leq}} = \begin{bmatrix} 0\,0\,0\,0\,1\,0\,0\,0\,0 \end{bmatrix}, \quad \mathbf{b_{leq}} = [0] \tag{152}$$

$$\mathbf{A_{eq}} = \begin{bmatrix} 0\,0\,0\,0\,0\,0\,1\,0\,0 \\ 0\,0\,0\,0\,0\,0\,0\,0\,1 \end{bmatrix}, \quad \mathbf{b_{eq}} = \begin{bmatrix} 0 \\ 0 \end{bmatrix} \tag{153}$$

Solving Eq. (130) using the weighted and the constraint matrices defined in Eqs. (146)–(153) yields a solution $\mathbf{p_{sol}}$, which are used to generate an initial estimate of the mastitis dynamics, for each experiment. This initial estimate is updated using the iterative approach discussed in Section 3.2.2 to improve the derivative initial condition estimation.

One hundred Monte Carlo simulations are conducted for the three noise experiments of Eqs. (143)–(145). Table 5 compares the 90% confidence interval of the identified parameters against the true values, for the weighting sets of (25,4,1) and (1,1,1). The identified parameters obtained with the (25,4,1) set are closer to the true values than those obtained with the (1,1,1) set. Table 6 gives the mean absolute error in the match of the three experiments in terms of the percentage. The maximum measured value is also given in the fourth column to provide a reference to these errors. Specifically relative to the maximum value the percentage errors are 1.0%, 1.6%, 2.1% for the (25,4,1) weightings and 1.6%, 2.6% and 3.5% for the (1,1,1) weightings. These results show that non-unity weights significantly improve parameter estimation and provide a better match to the data. Most importantly, the results show that this potential jet space is applicable to multiple experiments and still allows standard statistical approaches to data fitting like the weighted least squares to be utilized.

Note that if the Raue et al. [35] profile likelihood approach was used, it would involve 3 separate identifiability analyses involving many more simulations. In contrast the potential jet space method is a global method so the same formulation can be applied to all experiments.

3.2.4. Adaptive spacing

Consider the case where the experimental data from the non-linear mastitis model of Eqs. (119)–(121) is taken at times $\mathbf{t} = [0, 3, 6, 9, 12, 15, 20, 30, 40, 50, 60]^T$. For sensor noise, the additive Gaussian noise from the model of Eq. (95) is used.

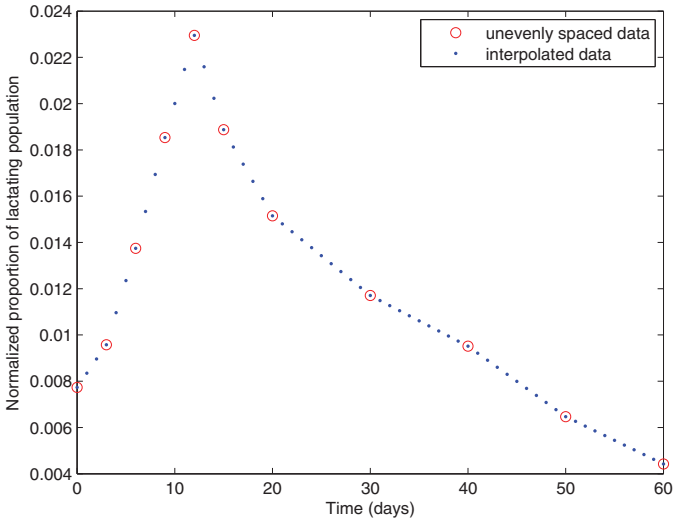

Fig. 11. Reported measurements for the case of sparser available data against interpolated noisy data.

Table 7
Comparing the identified parameters of the non-linear mastitis model, for the sparser data case, against the true parameters for 2%, 5% and 10% levels of noise.

Parameter	True value	Identified value (2%)	Identified value (5%)	Identified value (10%)
y_0	0.0075	[0.0072,0.0078]	[0.0069,0.0081]	[0.0061,0.0088]
dy_0	0.001	[0.0009,0.0011]	[0.0007,0.0013]	[0.0006,0.0014]
a	−2.3335	[−2.6677,−2.1488]	[−2.7379,−1.6401]	[−2.9876,−1.0522]
b	0.1500	[0.1439,0.1582]	[0.1120,0.1670]	[0.1081,0.1794]
d	0.0075	[0.0059,0.0077]	[0.0060,0.0080]	[0.0058,0.0093]

The uneven spacing of this experimental data is first made uniform by re-interpolating at 1 Hz, which represents measuring the infected population once a day as was done previously in the earlier results of Tables 3 and 4. Fig. 11 plots an example of the measurements (circles) for the measured sparser data and the interpolated noisy measurements (dots) for 10% noise.

The model and methods described in Section 3.2.2 are now applied to the re-interpolated noisy data of Fig. 11, for the cases of 2, 5 and 10% additive Gaussian noise. For each of these cases, 100 Monte Carlo simulations are performed for the nonlinear mastitis model of Eq. (127). Table 7 compares the 90% confidence interval of the identified lumped parameters of the non-linear mastitis model for the sparse data case, against the true parameters. The results show that the identified values are close to the true values, and are similar to the results in Table 3 where the raw measurements were taken every minute.

These results show that the sparser data and non-uniform spacing do not have a significant effect compared to more frequent uniform measurement for the potential jet space approach.

4. Conclusion

A potential jet space global identifiability theory was developed and applied to linear and non-linear compartmental models. For linear compartmental models, a matrix mapping method was presented for constructing the differential input–output equation, and the potential input–output equation of a system. It was shown that for identifiability theory, the two approaches are equivalent. However, the major advantage of the potential jet space approach is that the formulation is in terms of integrals so it is suitable for application on noisy data. To demonstrate this concept, the developed theory was first applied to analyze and identify a nitrous oxide uptake and

distribution. A noise analysis showed that the potential jet space was robust and useful for parameter identification, whereas the conventional differential jet space gave unbounded results in the presence of noise. The developed theory was also applied to simulated example of non-linear immunological model of mastitis in cows. For this system, the model integral formulation was iterated on the potential jet space to provide more accurate estimates of the initial conditions. Noise analysis showed that, for noise levels of up to 10%, the mean absolute errors are within 9% of the true values. Hence the global identifiability theory developed in this paper has been demonstrated to be very suitable for parameter identification of both linear and non-linear compartmental models in the presence of significant noise. It also has the ability to extract accurate initial conditions, that are not necessarily directly measurable, from noisy data and does not require simulations of the underlying model.

Appendix A. Proofs

Proof of Theorem 5 from Section 2.5.1.

Proof. Proof by induction. The base case of $n = 1$ in Eq. (48) follows immediately:

$$I^{(1)}(F(t)) = \int_0^t F(t)\,dt \equiv V^{0,1} \tag{A.1}$$

Suppose that Eq. (48) is true for $n = r$, where r is some integer:

$$I^{(r)}(F(t)) = \frac{1}{(r-1)!}\sum_{k=1}^{r}\binom{r-1}{k-1}(-1)^{k+1}t^{r-k}\int_0^t t^{k-1}F(t)\,dt \tag{A.2}$$

Consider the integral:

$$\int_0^t t^{m-k}\left(\int_0^t t^{k-1}F(t)\,dt\right)\,dt = \frac{t^{m-k+1}}{m-k+1}$$
$$\int_0^t t^{k-1}F(t)\,dt - \frac{1}{m-k+1}\int_0^t t^{m}F(t)\,dt \tag{A.3}$$

for $k, m \in \mathbb{N}^0$. Integrating Eq. (A.2) from 0 to t and using the integral of Eq. (A.3) yields:

$$I^{(r+1)}(F(t)) = \frac{1}{(r-1)!}\sum_{k=1}^{r}\binom{r-1}{k-1}(-1)^{k+1}\frac{t^{r-k+1}}{r-k+1}\int_0^t t^{k-1}F(t)\,dt + \frac{1}{(r-1)!}\sum_{k=1}^{r}\binom{r-1}{k-1}(-1)^{k+2}\frac{1}{r-k+1}\int_0^t t^{r}F(t)\,dt \tag{A.4}$$

Consider the following identities for $k, m \in \mathbb{N}^0$:

$$\frac{1}{m-k+1}\times\frac{1}{(m-1)!}\times\binom{m-1}{k-1} = \frac{1}{m!}\binom{m}{k-1} \tag{A.5}$$

$$\sum_{k=1}^{m}\binom{m}{k-1}(-1)^{k+2} = (-1)^{m+2} \tag{A.6}$$

Substituting Eqs. (A.5) and (A.6), and using the potential notation, Eq. (A.4) can be written in the form:

$$I^{(r+1)}(F(t)) = \frac{1}{r!}\sum_{k=1}^{r}\binom{r}{k-1}(-1)^{k+1}t^{r-k+1}V^{k-1,1} + \frac{1}{r!}(-1)^{r+2}V^{r,1} \tag{A.7}$$

$$= \frac{1}{r!}\sum_{k=1}^{r}\binom{r}{k-1}(-1)^{k+1}t^{r-k+1}V^{k-1,1} + \frac{1}{r!}\binom{r}{r+1-1}(-1)^{r+1+1}t^{r-(r+1)-1}V^{r,1}$$
$$\equiv \frac{1}{r!}\sum_{k=1}^{r+1}\binom{r}{k-1}(-1)^{k+1}t^{r-k+1}V^{k-1,1} \tag{A.8}$$

Hence Eq. (48) is true for $n = r + 1$ and therefore holds for all n. □

References

[1] T.K. Agasthi, Textbook of Anesthesia for Jaypee, Postgraduates Brothers Medical publishers Ltd., New Delhi, India, 2011.
[2] M. Anguelova, et al., Minimal output sets for identifiability, Math. Biosci. 239 (2012) 139–153.
[3] S. Ankinakatte, E. Norberg, P. Lovendahl, D. Edwards, S. Hojagaard, Predicting mastitis in dairy cows using neural networks and generalized additive models: a comparison, Electron. Agric. 99 (2013) 1–6.
[4] J. Armstrong, Principles of Forecasting: A Handbook for Researchers and Practitioners, Kluwer Academic Publishers, Norwell, MA, 2001.
[5] S. Audoly, G. Bellu, L. D'Angio, M.P. Saccomani, C. Cobelli, Global identifiability of nonlinear models of biological systems, IEEE Trans. Biomed. Eng. 48(1) (2001) 55–65.
[6] S. Audoly, L. D'Angio, M. Saccomani, C. Cobelli, Global identifiability of linear compartmental models—a computer algebra algorithm, IEEE Trans. Biomed. Eng. 45(1) (1998) 36–47.
[7] S. Bandara, J. Scloeder, R. Eils, H. Bock, T. Meyer, Optimal experimental design for parameter estimation of a cell signaling model, PLoS Comput. Biol. 5 (2009) 1–12.
[8] J.W. Barlow, L.J. White, R. Zadoks, Y. Schukken, A mathematical model demonstrating indirect and overall effects of lactation therapy targeting subclinical mastitis in dairy herds, Prev. Vet. Med. (2009) 31–42.
[9] R. Bellman, K.J. Astrom, On structural identifiability, Math. Biosci. 7 (1970) 329–339.
[10] G. Bellu, M.P. Saccomani, S. Audoly, L. D'Angio, Daisy: a new software tool to test global identifiability of biological and physiological systems, Comput. Methods Programs Biomed. 88 (2007) 52–61.
[11] F. Boulier, Differential elimination and biological modelling, Radon Ser. Comput. Appl. Math. 2 (2007) 111–139.
[12] B. Buchberger, An algorithmical criterion for the solvability of algebraic system of equation, Aeq. Math. 4(3) (1988) 45–50.
[13] J.G. Chase, et al., Adaptive bolus-based targeted glucose regulation of hyperglycaemia in critical care, Med. Eng. Phys. (2005) 1–11.
[14] P.M.S. Clark, C.N. Hales, How to measure plasma insulin, Diab. Metab. Res. (1994) 79–90.
[15] R.B. Colquitt, D.A. Colquhoun, R.H. Thiele, In silico modelling of physiologic systems, Best Pract. Res. Clin. Anaesthesiol. 25(4) (2011) 499–510.
[16] D. Doepfer, Recurrent clinical *Escherichia coli* mastitis in diary cows (Ph.D. thesis), Institute of Infectious Diseases and Immunology, Utrecht, the Netherlands, 2000.
[17] B.R. Faulkner, M.E. Campana, Compartmental model of nitrate retention in streams, Water Resour. Res. W02406 (2007) 1–8.
[18] H. Fouillet, et al., Compartmental modeling of postprandial dietary nitrogen distribution in humans, Am. J. Physiol. Endocrinol. Metab. 279 (2000) E161–E175.
[19] K. Godfrey, M.J. Chapman, Identifiability and indistinguishability of linear compartmental models, Math. Comput. Simulat. 32 (1990) 273–295.
[20] K.R. Godfrey, Compartmental Models and their Application, Academic Press, London and New York, 1983.
[21] A. Guyton, J. Hall, Textbook of Medical Physiology, 12th ed., Saunders, London, United Kingdom, 2010.
[22] C. Hann, J. Chase, J. Lin, T. Lotz, C. Doran, G. Shaw, Integral based parameter identification for long term dynamic verification of a glucose-insulin system model, Comput. Biol. Med. 77 (2005) 259–270.
[23] C. Hann, M. Hickman, Projective curvature and integral invariants, Acta Appl. Math. 74(2) (2002) 177–193.
[24] F. He, M. Brown, M. Yue, Maximin and Bayesian robust experimental design for measurement set selection in modelling biochemical regulatory systems, Int. J. Robust Nonlinear Control 20 (2010) 1059–1078.
[25] V. Ivancevic, T. Ivancevic, Applied Differential Geometry: A modern Introduction, World Scientific Publishing, Singapore, 2007.
[26] M. Jirstrand, Algebraic methods for modeling and design in control (Ph.D. thesis), Linkoping University, Linkoping, Sweden, 1996.
[27] An efficient method for structural identifiability analysis of large dynamic systems, Proceedings of the 16th IFAC Symposium on System Identification, 2012.
[28] L. Ljung, T. Glad, On global identifiability for arbitrary model parameterization, Automatica 30(2) (1990) 265–276.
[29] P. Macheas, A. Iliadis, Modeling in Biopharmaceutics, Pharmacokinetics, and Pharmacodynamics: Homogeneous and Heterogeneous Approaches, Springer-Verlag, New York, 2006.
[30] E.L. Mansfield, P.A. Clarkson, Applications of the differential algebra package diffgrob2 to classical symmetries of differential equations, J. Symbolic Comput. 23 (1997) 517–525.
[31] G. Margaria, E. Riccomagno, M. Campbell, H. Wynn, Differential algebra methods for the study of the structural identifiability of rational function state-space models in the biosciences, Math. Biosci. 19 (2001) 1–26.
[32] N. Meshkat, M. Eisenberg, J.J.D. Stefano, An algorithm for finding globally identifiable parameter combinations of nonlinear ode models using groebner bases, Math. Biosci. 222 (2009) 61–72.
[33] P.J. Olver, Differential invariants, Acta Appl. Math. 41 (1995) 271–284.
[34] H. Pohjanpalo, System identifiability based on power-series expansion of solution, Math. Comput. Simulat. 41 (1978) 21–33.
[35] A. Raue, et al., Structural and practical identifiability analysis of partially observed dynamical models by exploiting the profile likelihood, Bioinformatics 25 (2009) 1920–1929.
[36] A. Raue et al., Comparison of approaches for parameter identifiability analysis of biological systems, Bioinformatics (2014) 1440–1448.

[37] A. Sedoglavic, A probabilistic algorithm to test local algebraic observability in polynomial time, J. Symbolic Comput. 33 (2002) 735–755.
[38] G. Tanner, Pharmacokinetics of inhalation anesthetics: a three-compartment linear model, Anesth. Analg. 61(7) (1982) 587–594.
[39] E. Walter, Identifiability of State Space models, Springer-Verlag, Berlin, 1982.
[40] E. Walter, Y. Lecourtier, Unidentifiable compartmental models: what to do? Math. Biosci. 56 (1981) 1–25.
[41] E. Walter, L. Pronzato, Identification of Parametric Models from Experimental Data, Springer, Masson, 1997.
[42] G. Wells, H. Prest, C.R. Signal, IV, noise and detection limits in mass spectrometry, a technical note, Technical Notes, Agilent Technology, 2011, pp. 1–5.
[43] J.W.T. Yates, Structural identifiability of physiologically based pharmacokinetic models, J. Pharmacokinet. Pharmacodyn. 33(4) (2006) 421–439.
[44] P. Young, Parameter estimation for continuous-time models—a survey, Automatica 17 (1981) 23–39.